NIPER-510
Distribution Category UC-122

MODELING OF SURFACTANT TRANSPORT AND ADSORPTION IN POROUS MEDIA

Topical Report

NIPER--510

DE91 002230

By
Frank T. H. Chung

April 1991

Work Performed Under Cooperative Agreement No. DE-FC22-83FE60149

Prepared for
U.S. Department of Energy
Assistant Secretary for Fossil Energy

Jerry Casteel, Project Manager
Bartlesville Project Office
P.O. Box 1398
Bartlesville, OK 74005

Prepared by
IIT Research Institute
National Institute for Petroleum and Energy Research
P. O. Box 2128
Bartlesville, OK 74005

MASTER

DISTRIBUTION OF THIS DOCUMENT IS UNLIMITED

DISCLAIMER

This report was prepared as an account of work sponsored by an agency of the United States Government. Neither the United States Government nor any agency thereof, nor any of their employees, makes any warranty, express or implied, or assumes any legal liability or responsibility for the accuracy, completeness, or usefulness of any information, apparatus, product, or process disclosed, or represents that its use would not infringe privately owned rights. Reference herein to any specific commercial product, process, or service by trade name, trademark, manufacturer, or otherwise does not necessarily constitute or imply its endorsement, recommendation, or favoring by the United States Government or any agency thereof. The views and opinions of authors expressed herein do not necessarily state or reflect those of the United States Government or any agency thereof.

This report has been reproduced directly from the best available copy.

Available to DOE and DOE contractors from the Office of Scientific and Technical Information, P.O. Box 62, Oak Ridge, TN 37831; prices available from (615)576-8401, FTS 626-8401.

Available to the public from the National Technical Information Service, U.S. Department of Commerce, 5285 Port Royal Rd., Springfield, VA 22161.

TABLE OF CONTENTS

Page

Abstract 1

Introduction 1

Acknowledgments 5

Modeling Development 5

1. Convection-Dispersion (CD) Model 6
2. Convection-Dispersion-Capacitance (CDC) Model 7
3. Convection-Dispersion-Adsorption (CDA) Model 9
4. Convection-Dispersion-Adsorption-Capacitance (CDAC) Model 11
5. One-Dimensional Radial Flow Model 13
6. Numerical Solution Method 14
7. Parameter Determination 17
8. Influence of Parameters 18

Experiments 21

1. Experimental Procedure 21
2. Results and Discussion 22

Summary and Conclusions 26

References 27

Appendix A—Dimensionless Equations and Characteristic Parameters 30

A. General CDAC Model 30
B. CDA Model 31
C. CDC Model 31
D. CD Model 31
E. Radial Flow Model 32

Appendix B—Numerical Solution for the CDAC Model 33

Appendix C—Batch Experimental Results 35

ILLUSTRATIONS

1. Outline of modeling foam flow in porous media 2
2. Adsorption behavior for surfactant adsorption on mineral oxide surfaces 5
3. Effect of dispersion on effluent concentration profiles (CD model) 7
4. Effects of dispersion and capacitance on effluent concentration profiles (CDC model) 9
5. Effects of adsorption on effluent concentration profiles at constant dispersion (CDA model) 10

ILLUSTRATIONS—Continued

Page

6. Effects of both dispersion and adsorption capacity on effluent concentration profiles (CDA model) 11
7. Effluent concentration profiles of Langmuir equilibrium model and dynamic adsorption model 12
8. Physical model for the CDAC model 12
9. Physical model of radial core 14
10. Fitted results for CDC model with Coats and Smith data 15
11. Fitted results for CDC model with Baker data 16
12. Effluent concentration of surfactant (AOS C1618) through 30-cm-long Berea core and the fitted Langmuir model 16
13. Effects of capacitance dispersion and adsorption on effluent concentration profile 19
14. Surfactant concentration profiles in the flowing space and the stagnant space of a 2-ft-long core 20
15. Surfactant concentration profiles in the flowing space and the stagnant space of a 2-ft radius radial-flow core 20
16. Experimental apparatus 22
17. Effluent concentration profiles for the surfactant flowing through a 2-ft-long sand-packed column 23
18. Concentration profiles for the surfactant flowing through a 2-ft-long sand-packed column 23
19. Concentration profiles for the surfactant flowing through a 1-ft-long sand-packed column 25
20. Effluent Alipal CD-128 concentration profile during continuous injection 25
21. Results of Alipal CD-128 effluent concentration from different analysis methods during continuous injection 26

C-1. Adsorption isotherm for Alipal CD-128 on Berea sand 35
C-2. Alipal CD-128 loss on various media 36
C-3. Effect of pH on Alipal CD-128 adsorption on kaolinite 37
C-4. Alkaline effect of Alipal CD-128 adsorption on kaolinite 37

MODELING OF SURFACTANT TRANSPORT AND ADSORPTION IN POROUS MEDIA

by

Frank T. H. Chung

ABSTRACT

Surfactant concentration is one of the important factors in determining foam generation and propagation. When surfactant solution is flowing in a reservoir formation, surfactants will be diluted by flow dispersion, retained in dead-end pores, adsorbed on rock surfaces, or precipitated due to ion exchange. All these physical and chemical aspects complicate the problem of foam. The loss of surfactant will be detrimental to the performance of gas foam. Information of surfactant concentration profiles in reservoir formations is essential for gas foaming technique development. This research was designed to investigate the transport and adsorption phenomena of surfactants in porous media.

The major objective of this research is to investigate with mathematical models the transport and dynamic adsorption of surfactants in porous media. The mathematical models have taken into account the convection, dispersion, capacitance, and adsorption effects on concentrations of surfactants. Numerical methods and computer programs have been developed which can be used to match experimental results and to determine the characterization parameters in the models. The models can be included in foam simulation programs to calculate surfactant concentration profiles in porous media.

A flow experimental method was developed to measure the effluent surfactant concentration, which will be used to determine the model parameters. Commercial foaming agent Alipal CD-128 was used in this study. Equilibrium adsorption and surfactant precipitation have been tested. Tracer solutions with a nonadsorbing solute such as dextrose and sucrose were used to determine the dispersion parameters for the experimental sandpack; thus, the adsorption of the surfactant in the test sand can be identified with an adequate model.

INTRODUCTION

Gas flooding is an effective enhanced oil recovery (EOR) method. The displacement efficiency of gas flooding can be economically feasible under both miscible and immiscible conditions. The efficiency of gas flooding has been hindered by the unfavorable mobility of injected gases as well as gravity segregation, which results in poor sweep efficiency. Several methods have been considered to mitigate the problem of mobility control: (1) water-alternating gas (WAG) process; (2) use of surfactants to generate foam to reduce gas mobility; (3) polymer-enhanced WAG process; (4) viscosifying the gas phase by means of addition of polymers as direct thickeners; (5) in situ polymerization of soluble monomers in

means of addition of polymers as direct thickeners; (5) in situ polymerization of soluble monomers in supercritical CO_2; and (6) adding cosolvents in supercritical CO_2 to enhance extraction power and to viscosify the gas phase.

Interest in the use of foams has resulted from their potential application as mobility-control agents for improving oil recovery in EOR processes. Although the foam technique for gas mobility control has been successfully tested in laboratory core flooding experiments, the application of foam in field gas EOR is still in its primary stages, primarily because of the lack of adequate models or scaling rules to describe its behavior. Several technical papers on studies of foam flow behavior in porous media have been published . However, most of the papers deal only with phenomenological descriptions of foam behavior in laboratory-scale models. Research is needed on the development of quantitative relationships of foam behavior, rather than qualitative description. Some progress in the development of prototype models describing foam flow behavior in porous media has been made.[1-2] Figure 1 illustrates the modeling

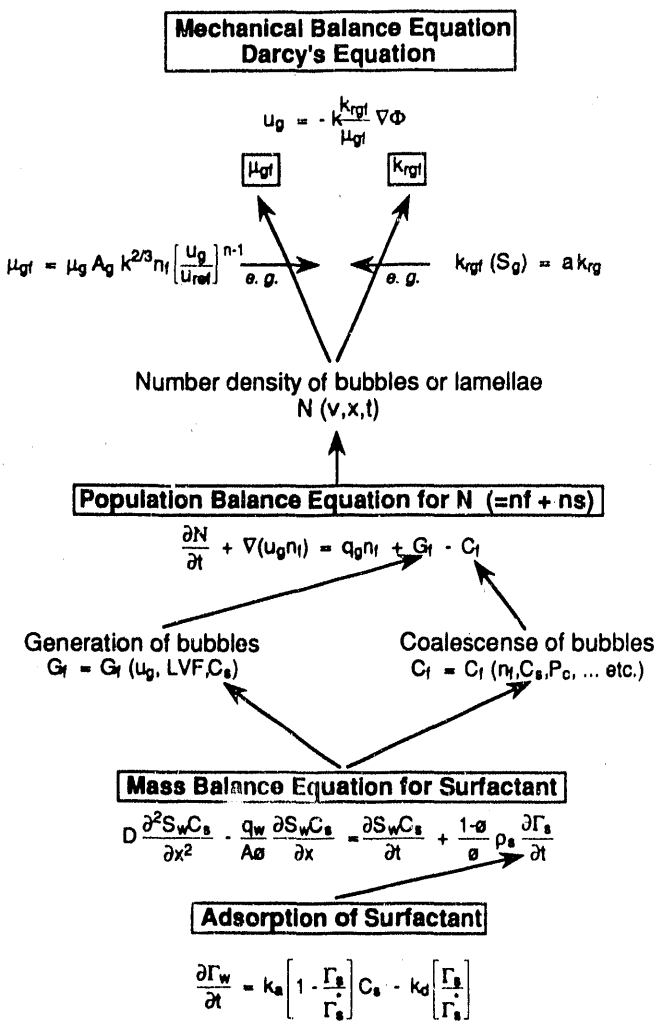

FIGURE 1. - Outline of modeling foam flow in porous media.

hierarchy. The approach employs Darcy's equation with modifications introduced in the terms of relative permeability and viscosity by the effect of foam on gas flow in porous media. This simplified approach provides a framework to develop a model that is computationally convenient and useful. Both the apparent foam viscosity and the effective gas relative permeability depend on foam texture.[1-3] The bubble size distribution, or equivalently the foam texture, is a controlling factor for the rheological properties of foam. The number density of foam bubbles or lamella is dependent on the generation and coalescence of the bubbles through the population balance equation.[1] The mechanisms of foam generation and coalescence is then dependent on surfactant concentration, capillary pressure, gas flow rate, and other factors. The adsorption of the surfactant comes into play in the mass balance equation for the surfactant. The mass balance equation for the surfactant, in turn, dictates the availability of the surfactant to generate foam.

NIPER's previous work on this project was devoted to the study of foam rheology and effective foam relative permeability, and results were published.[4] This work is designed to study the transport and adsorption phenomena of surfactants in porous media and to develop mathematical models for the prediction of surfactant concentration distribution.

One of the major problems encountered in injecting surfactants in reservoirs is the adsorption of surfactants in formation rock, which consumes most of the injected surfactants. The loss of surfactants due to adsorption and precipitation will reduce performance and make surfactant applications uneconomical. To design and optimize a surfactant injection process, the transport and adsorption phenomena of the injected surfactants in porous media must be understood. The transport and adsorption of surfactants in reservoir formations are complicated problems. These problems are briefly reviewed in the following paragraphs.

Surfactants are complicated chemicals which contain hydrophobic and hydrophilic parts. The hydrophilic groups are usually polar or ionic, whereas the hydrophobic parts are usually long-chain nonpolar hydrocarbons. The two different types of interaction: ion-ion interaction and hydrophobic interaction complicate the surfactant solution properties. Surfactant molecules will aggregate to form micelles when the concentration of surfactant is above the critical micellar concentration (CMC) of the surfactant. Micelles do not adsorb significantly.[5] Adsorption of surfactant molecules has various configurations. The configuration of surfactant molecules in the adsorbed phase is different from that of the bulk fluid phase. Surfactant molecules may aggregate on the adsorbed phase to form two-dimensional hemimicelles due to lateral attractions (hydrophobic interaction) between adsorbed surfactants. Surfactant monomers in solution are simultaneously in equilibrium with both micelles and adsorbate.

Reservoir fluids include oil, brine, and gases. Surfactant-brine solution is an electrolyte system whose properties are difficult to predict. Data on the ionic composition of reservoir connate water indicate a large amount of dissolved mineral ions such as Na^+, Ca^{++}, and Mg^{++}. Interaction of these ions with

anionic surfactant can produce precipitation.[6-7] Also, the mixing of surfactants with reservoir fluids in porous media can generate other complicated phases such as emulsions and foam.

Formation rocks are heterogeneous. Reservoir minerals include various chemicals such as silicates, carbonates, halides, sulfides, and sulfates; therefore, reservoir rock surfaces can be assumed to be composed of patches with different surface energies. Theoretical work for evaluating surface heterogeneity has been developed based on the so-called "patchwise model."[8-9] Investigation of surfactant adsorption in reservoir formations requires knowledge of the various types and amounts and positioning of minerals in rock matrix and in pore channels. In addition, rock surfaces are not smooth. Part of the surface area is inside micro-pores with diameters of molecular size. Like molecular sieves, surfactant molecules may not be able to penetrate into some smaller pores and be in contact with rock surfaces. It has been found that the surface of a porous formation is a fractal dimension[10] where the surface area of the porous formation rock will be related to the fluid molecular size; thus, the surface area determined by the standard BET method may not be the effective area for surfactant adsorption.

Commercial surfactant products are not isometrically pure. They are usually mixtures of surfactants and cosurfactants such as alcohols. Some of the observed results for the adsorption of surfactant mixtures show maxima and minima in the isotherms, which may be due to complex surfactant component interactions.[5] For basic studies, it is desirable to simplify the problem by using pure surfactants and minerals. Even for such a simplified case, the adsorption isotherm is still complicated. Figure 2 shows a typical adsorption isotherm for surfactant on mineral oxide surfaces. The isotherm can be divided into four regions. In Region I, only unassociated, first-layer molecules are present, and the adsorption obeys Henry's law. In Region II, aggregates on the surface are beginning to form hemimicelles, and adsorption increases more rapidly. In Region III, the adsorption increases slowly and eventually reaches the plateau region (Region IV). The transition point for adsorption to reach the plateau was found to correspond to the CMC of the surfactant.[5] These phenomena have been observed in many surfactant adsorption studies.[5,11] This shape of adsorption isotherms cannot be described by those homogeneous surface models such as the Langmuir model, the BET model, and Henry's law. Scamehorn et al.[5] have developed a patchwise adsorption model, which incorporates bilayer adsorption, lateral interactions, and two-dimensional phase transitions. The model describes isotherms observed below the CMC; however, this model still oversimplifies surfactant solutions by assuming an ideal solution.

Because of the importance of surfactant adsorption to chemical EOR, extensive basic research on the adsorption of surfactants has been conducted under the sponsorship of the U.S. Department of Energy. Most of the adsorption studies have been on equilibrium adsorption. Seldom have these studies been conducted on dynamic adsorption at flowing conditions.[12-13] Surfactant concentration is a critical factor to foam generation. Surfactant distribution in porous media is affected by adsorption and

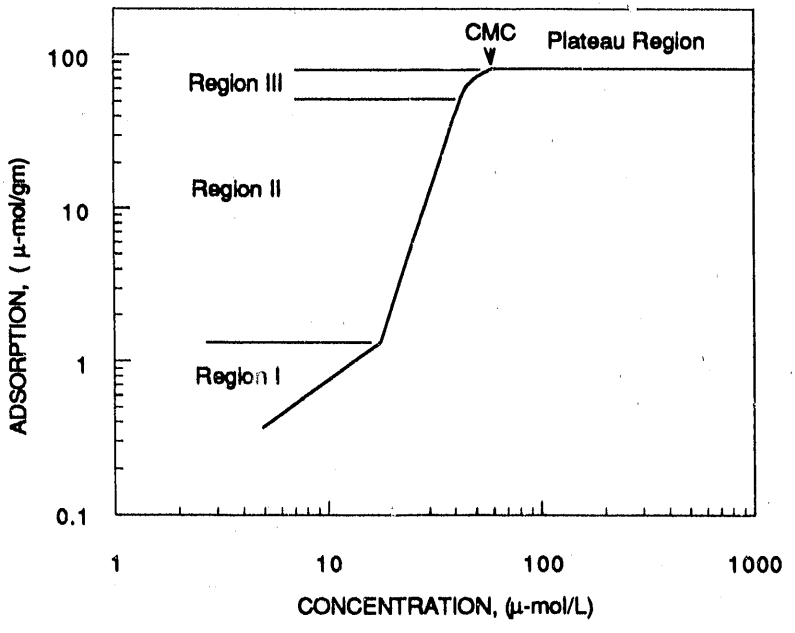

FIGURE 2. - Adsorption behavior for surfactant adsorption on mineral oxide surfaces.

other factors such as dispersion and capacitance-retention. Trogus et al.[12] first conducted a dynamic adsorption study for anionic and nonionic surfactant flow through Berea cores. Their results show that surfactant adsorption is dynamic under flow conditions. They also presented a model to describe the kinetics of adsorption.

The objective of this work was to study the transport and adsorption phenomena for foaming surfactants in porous media and to develop a model to describe these phenomena. The project work includes mathematical modeling and experiments.

ACKNOWLEDGMENTS

This work was sponsored by the U.S. Department of Energy under cooperative agreement DE-FC22-83FE6-0149. The author wishes to thank Clarence Raible, Randall Louvier, and Bonnie Gall of NIPER for their contribution to this project.

MODELING DEVELOPMENT

Transport of chemicals in porous media has been studied in petroleum engineering, chemical engineering, ground-water pollution engineering, and soil physics. It has been recently studied with reference to chemical flooding in enhanced oil recovery (EOR). Multicomponent single-phase flow through porous media is found in many EOR processes: surfactant flooding, alkaline flooding, polymer flooding, and microbial flooding. An important design criterion for chemical injection is the slug size that is

required for optimum oil recovery. The transport of injected chemicals or microorganisms is governed by many physical and chemical aspects such as convection, dispersion, adsorption, capacitance-retention, pore-throat filtration, and chemical reaction.

This study was focused on the propagation of surfactant solutions in porous media. The purpose of injection of surfactant solutions into reservoir formations is to generate gas foam for gas flow control. The foam flow problem is much more complicated because it deals with multicomponent and mutliphase flow through heterogeneous porous media. To model foam generation and flow in reservoir formations, the surfactant solution flow in porous media should first be modeled.[1-2,4] To simplify the problem, in this work, the model was assumed to be a multicomponent single-phase flow with constant flow rate, and the surfactant distribution was assumed to be affected by dispersion, capacitance-retention, and adsorption. The porous medium was assumed to be homogeneous. A one-dimensional linear flow and radial flow models were developed in this work.

1. Convection-Dispersion (CD) Model

The simplest model to describe the miscible transport of chemicals through a reservoir rock is the convection-dispersion (CD) model which considers only the dispersion effect on the chemical concentration profile. The model equation is characterized by one dimensionless parameter, the Peclet number $P_e(=VL/D)$. The differential equation of the model is

$$D\frac{\partial^2 C}{\partial x^2} - \frac{q}{A\phi}\frac{\partial C}{\partial x} = \frac{\partial C}{\partial t} \qquad (1)$$

where C is the chemical concentration, D is the mass dispersion coefficient, q the volume flow rate, A is the cross section area, ϕ is the porosity, x is the linear distance from 0 to L, and t is the time scale. The interstitial velocity, $V(= q/A\,\phi)$, is constant.

The analytical solutions for various boundary conditions are well known.[14] The effluent concentration profiles of this model are nearly symmetrical around the breakthrough of 50% of the injection concentration. Figure 3 is a typical breakthrough curve of the effluent concentration. The 50% concentration appears at the outlet when 1 PV is injected. The parameter-Peclet number characterizes the dispersion of the concentration profile curve. When Peclet equals infinity (i.e., no dispersion), the flow becomes a plug flow. It has been shown that molecular diffusion, mass tortuosity, and mechanical mixing contribute to the mass dispersion coefficient D. A relationship for the mass dispersion coefficient was proposed as[15]

$$D = D_m(1+\tau_m) + a(V)^{\alpha} \qquad (2)$$

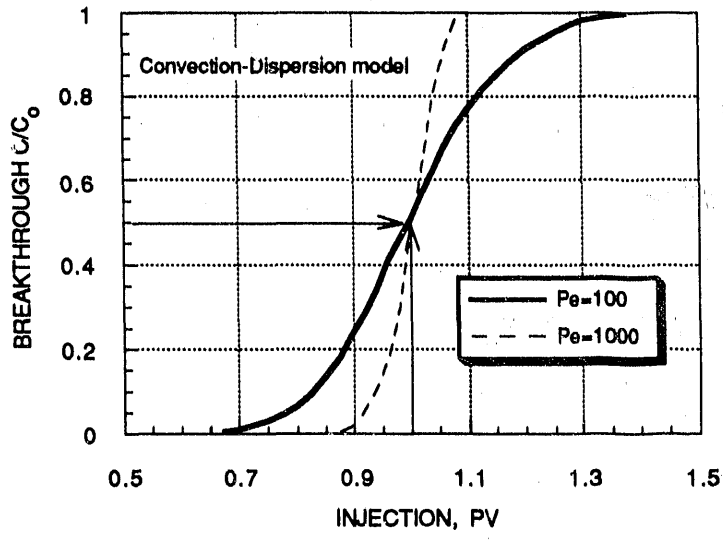

FIGURE 3. - Effect of dispersion on effluent concentration profiles (CD model).

where D_m is molecular diffusion coefficient, τ_m is mass tortuosity, a is a constant, and α is a parameter which is between 1 and 2.[16] Several studies performed on consolidated packed beds and Berea sandstone show α to be approximately 1.25.[17-19]

The model is suitable for the case such as the injection of aqueous solutions with a nonadsorbing soluto such as sucrose into a sand-packed column, where adsorption and dead-end effects can be ignored. Sucrose has been injected with surfactants as a tracer to determine the mass transfer coefficient for the injected surfactant.

2. Convection-Dispersion-Capacitance (CDC) Model

Many experiments of coreflooding exhibit asymmetry of the effluent concentration profile. Because the dead-end pores have occupied some void space, the actual void space for flow phase is less than the actual pore volume. Therefore, the breakthrough of the 50% concentration occurs significantly before 1 PV is injected.[20-21] To describe this phenomenon, Coats and Smith[14] proposed the convection-dispersion-capacitance (CDC) model. This model considers a zone of stagnant fluid which exchanges mass with the mobile fluid. The model has three parameters: Peclet number (Pe), the fraction of pore volume occupied by mobile fluid (f), and the dimensionless Stanton number (S_t=kL/v) which relates mass transfer (between mobile and stagnant fluids) and convection. The differential equations of this model are given as

$$D\frac{\partial^2 C}{\partial x^2} - \frac{q}{A\phi}\frac{\partial C}{\partial x} = f\frac{\partial C}{\partial t} + (1-f)\frac{\partial C^*}{\partial t} \qquad (3)$$

$$(1-f)\frac{\partial C^*}{\partial t} = k\,(C - C^*) \tag{4}$$

where C^* is the concentration in the stagnant space and k is the mass transfer coefficient between the mobile fluid and the stagnant fluid. This model has been used to determine the dead-end space of a core from the shift of the breakthrough of 50% concentration point. Solution of equations 3 and 4 depends on boundary conditions. Several different types of boundary conditions have been proposed.[14, 22] The following two types of boundary conditions (B.C.) are more reasonable for this model,

B.C. 1 - for finite medium[23]

$$VC_o = VC - D\frac{\partial C}{\partial x} \qquad \text{at } x = 0 \tag{5}$$

$$\frac{\partial C}{\partial x} = 0 \qquad \text{at } x = L \tag{6}$$

B.C. 2 - for semi-infinite medium[16]

$$VC_o = VC - D\frac{\partial C}{\partial x} \qquad \text{at } x = 0 \tag{7}$$

$$C \rightarrow 0 \qquad \text{at} \qquad x \rightarrow \infty \tag{8}$$

B.C. 2, which includes an exit boundary condition as $x \rightarrow \infty$, is appropriate for solving the differential equation analytically, but it cannot be explicitly imposed to solve the finite difference forms of the equations of the CDC model. An analytic solution for the CDC model with B.C. 2 was given by Coats and Smith.[14] Numerical solution was developed for equations 3 and 4 with B.C. 1. The behavior of the model is shown in figure 4 for different sets of parameters. The breakthrough curve comes out earlier as the value of f decreases, and increasing the mass transfer rate (S_t number) will make the effluent concentration profile tailing.

The CDC model has been used extensively in the petroleum industry for quantifying dispersion and tailing in consolidated porous media. Jasti et al.[24] performed coreflood experiments using radioactive tracers to investigate the capacitance effects on tracer tailing. They found that tracer tailing is a function of the ratio of the molecular diffusivity to the flow rate. Their study also indicated that the CDC model displays realistic residence time distribution behavior for tracer. However, caution should be exercised in fitting the parameters: f and k. The flowing fraction f should be independent of the interstitial velocity. The CDC

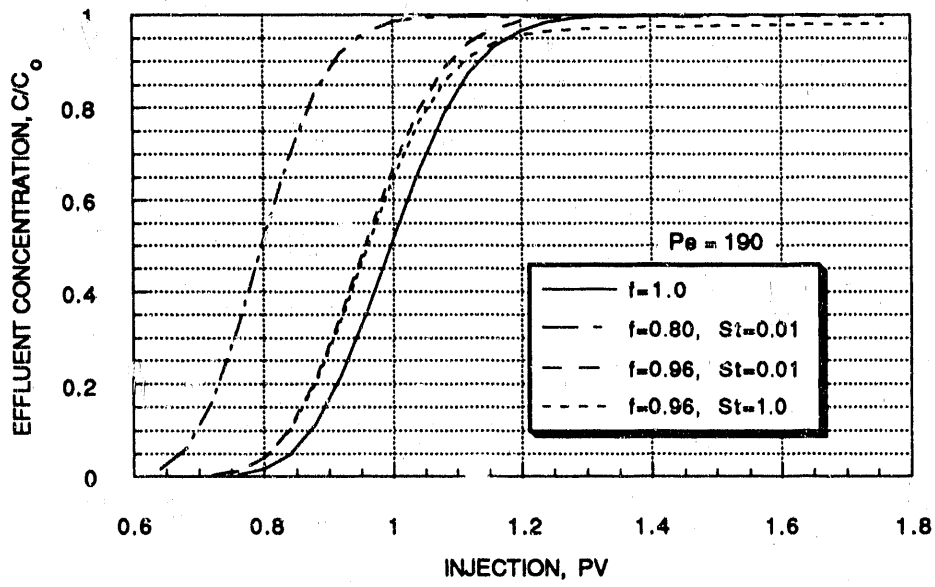

FIGURE 4. - Effects of dispersion and capacitance on effluent concentration profiles (CDC model).

model has also been applied for multiphase flow in porous media. Salter and Mohanty[25] studied two-phase flow, where tracers were added to both the wetting and nonwetting phases. The effluent tracer profiles from coreflood experiments were fitted with a modified four-parameter CDC model, which divides each phase into three fractions: flowing, dendritic, and isolated.

3. Convection-Dispersion-Adsorption (CDA) Model

In addition to the effect of capacitance, adsorption will delay the effluent profile: the breakthrough of the 50% concentration occurs after 1 PV is injected. To interpret this experimental fact, several authors[9,36-37] presented the convection-dispersion-adsorption (CDA) model. The adsorption term has been usually modelled by the Langmuir isotherm which assumes instantaneous equilibrium compared with the rate of convection and dispersion.[36] But Trogus et al.[9] observed dynamic adsorption for commercial surfactants and have proposed a kinetic adsorption model for surfactant adsorption. A general model which employed the dynamic adsorption model was given as[15, 27]

$$D\frac{\partial^2 C}{\partial x^2} - \frac{q}{A\phi}\frac{\partial C}{\partial x} = \frac{\partial C}{\partial t} + \frac{A_s}{\phi}\frac{\partial C_s}{\partial t} \tag{9}$$

$$\frac{\partial C_s}{\partial t} = k_a(Q_s - C_s)C - k_d C_s \tag{10}$$

where C_s is the chemical concentration on the solid surface (per unit surface area), A_s is the rock interstitial area per unit volume (total volume), Q_s is the total adsorption capacity of the adsorbent, and k_a and k_d are adsorption and desorption rate constants, respectively. The surfactant concentration of the injected solution is C_o. The CDA model which has four dimensionless parameters: Peclet number (Pe), adsorption capacity number ($L_a=A_sQ_s/\Phi C_o$), flow rate number ($J=V/Lk_aC_o$), and kinetic adsorption number ($E=k_d/k_aC_o$), does not consider the retention of chemicals in dead-end pores. Ramirez et al.[15] conducted single-phase sucrose-tracer displacement tests on a fired Berea core with permeability of 810 md and porosity of 22%. Their results show that for fired Berea the dead-space volume is very small (approximately 3%), and the capacitance effects are negligible. The dimensionless form of equations 9 and 10 are given in appendix A. There is no analytical solution for the set of nonlinear differential equations with the boundary conditions of equations 5 and 6. Different numerical techniques have been used to solve the set of equations. The Barakat-Clark finite-difference method[28] was used by Satter et al.,[27] and the Crank-Nicolson finite difference method[29] was used by Ramirez et al.[15] The effluent concentration profiles of the model are shown in figure 5. The profiles are delayed by adsorption. By lowering the kinetic adsorption number (E), i.e., lowering the desorption rate relative to the adsorption rate, will retain the chemical inside the porous media and thus make asymmetric tailing of effluent concentration profiles. The effects of the adsorption capacity number (La) with the Peclet number (Pe) on the effluent concentration profile are shown in figure 6.

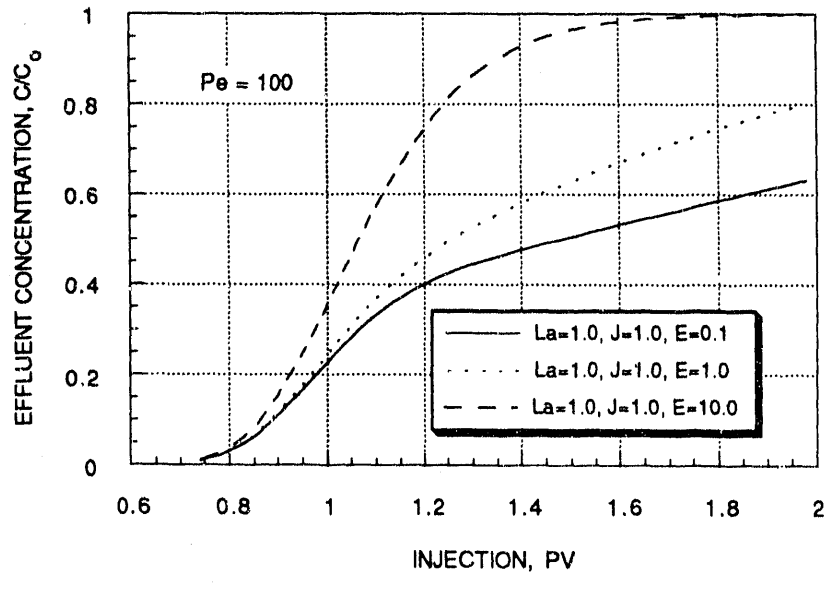

FIGURE 5. - Effects of adsorption on effluent concentration profiles at constant dispersion (CDA model).

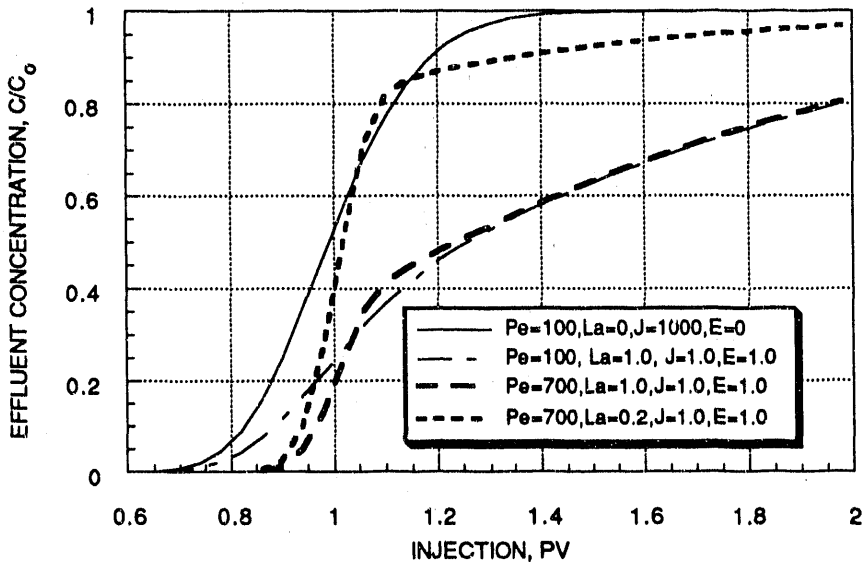

FIGURE 6. - Effects of both dispersion and adsorption capacity on effluent concentration profiles (CDA model).

For the case that adsorption and desorption reach equilibrium instantaneously, equations 9 and 10 can be combined as[27]

$$D\frac{\partial^2 C}{\partial x^2} - \left(\frac{q}{A\phi}\right)\frac{\partial C}{\partial x} = \left[1 + \frac{A_s a}{\phi(1+bC)^2}\right]\frac{\partial C}{\partial t} \tag{11}$$

where a ($=k_a Q_s/k_d$) and b ($=k_a/k_d$) are constants in Langmuir adsorption isotherm. The behavior of this equilibrium adsorption model is shown in figure 7 as compared with time-depend adsorption model (eq. 10).

4. Convection-Dispersion-Adsorption-Capacitance (CDAC) Model

A general model which takes into account convection, dispersion, adsorption, and capacitance mechanisms was proposed by Bidner and Vampa.[30] The model contains all six dimensionless parameters: Pe, S_t, f, La, E, J, already mentioned in the previous models. The physical model is illustrated in figure 8.

For a one-dimensional single-phase flow through porous media, the model encompasses the following differential equations,

(1) Macroscopic balance equation for chemical in flowing space

$$D\frac{\partial^2 C}{\partial x^2} - \frac{q}{A\phi}\frac{\partial C}{\partial x} = f\left(\frac{\partial C}{\partial t} + \frac{A_s}{\phi}\frac{\partial C_s}{\partial t}\right) + (1-f)k(C - C^*) \tag{12}$$

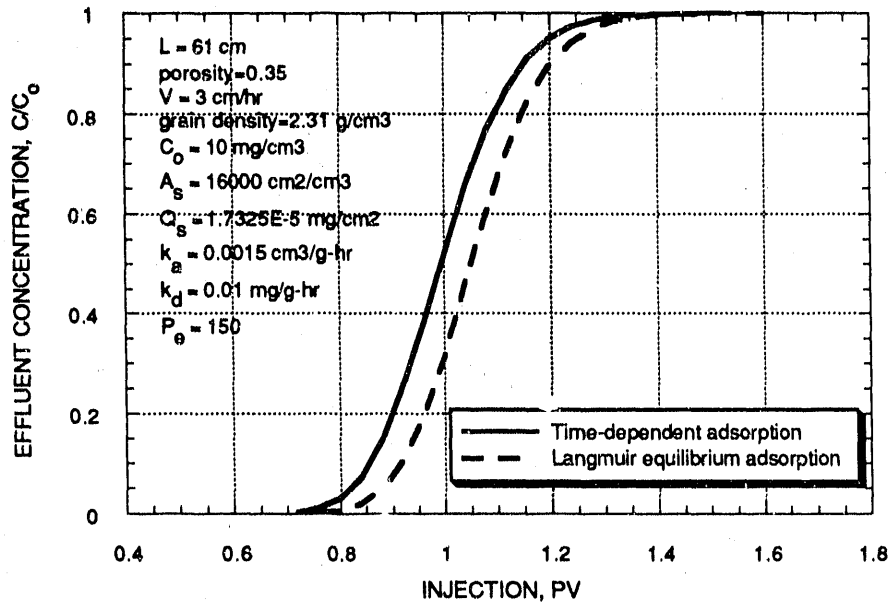

FIGURE 7. - Effluent concentration profiles of Langmuir equilibrium model and dynamic adsorption model.

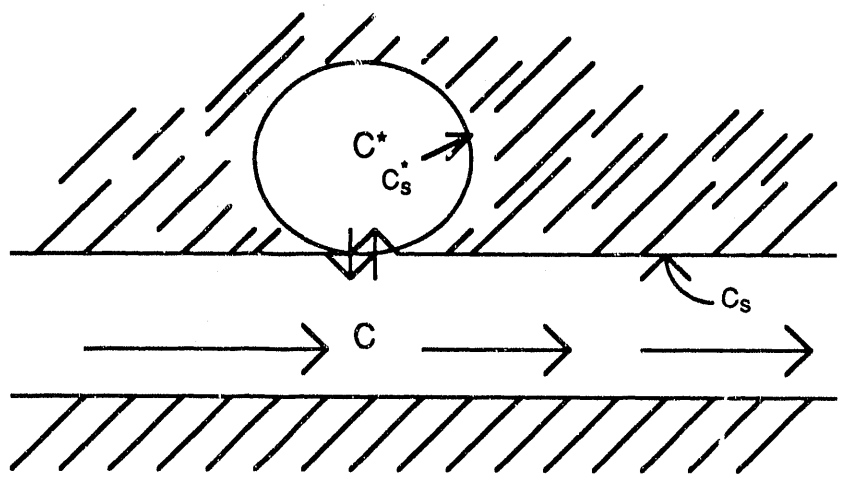

FIGURE 8. - Physical model for the CDAC model.

(2) Mass transfer between the flowing space and the stagnant space

$$k(C - C^*) = \frac{\partial C^*}{\partial t} + \frac{A_s}{\phi}\frac{\partial C_s^*}{\partial t} \tag{13}$$

(3) Adsorption kinetic on the surface of flowing space

$$\frac{\partial C_s}{\partial t} = k_a C(Q_s - C_s) - k_d C_s \tag{14}$$

(4) Adsorption kinetic on the surface of stagnant space

$$\frac{\partial C_s^*}{\partial t} = k_a C^*(Q_s - C_s^*) - k_d C_s^* \tag{15}$$

where C_s^* is the concentration of chemical adsorbed on the surface in the stagnant space. All other symbols are the same as previous models.

The general CDAC model can be reduced to the above-mentioned models: CD, CDC, and CDA. When there is no adsorption, i.e., $C_s = C_s^* = 0$, the CDAC model reduces to the Coats-Smith's CDC model of equations 3 and 4. If the flowing fraction f is equal to 1, the CDAC model reduces to the CDA model of equations 9 and 10. If there is no adsorption and stagnant space, the CDAC model will reduce to the CD model of equation 1. The dimensionless forms of the CDAC model and other models are given in appendix A.

5. One-Dimensional Radial Flow Model

The general CDAC model can be converted to a one-dimensional radial flow model This model could be applied to the radial core experiment or near-wellbore case to predict surfactant concentration near wellbore. The physical model is shown in figure 9.

Under the assumptions of homogeneous porous medium and constant injection rate, the macroscopic balance equation for surfactant solution can be written as

$$D\left[\frac{1}{r}\frac{\partial}{\partial r}\left(r\frac{\partial C}{\partial r}\right)\right] - V(r)\frac{\partial C}{\partial r} = f\left[\frac{\partial C}{\partial t} + \frac{A_s}{\phi}\frac{\partial C_s}{\partial t}\right] + (1-f)\left[\frac{\partial C^*}{\partial r} + \frac{A_s}{\phi}\frac{\partial C_s^*}{\partial t}\right] \tag{16}$$

and the microscopic balance equations are the same as equations 13 to 15. The boundary conditions are changed to

At $r = r_o$, for $t > 0$

$$V_o C - V_o C_o = D\frac{\partial C}{\partial r} \tag{17}$$

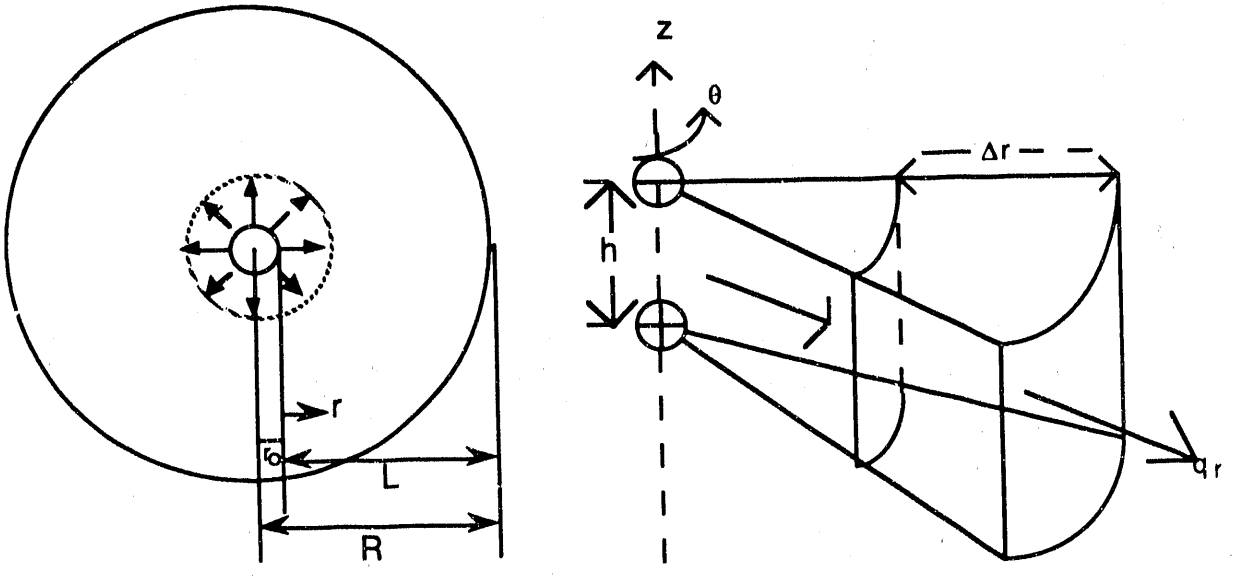

FIGURE 9. - Physical model of radial core.

At r = R, for t > 0

$$\frac{\partial C}{\partial r} = 0 \tag{18}$$

where V_o, the flow velocity at the wellbore inlet, is constant and all other notations are the same as the linear CDAC model except the macroscopic balance equation is written in cylindrical coordination (r, θ, Z). Since the porous medium is homogeneous in porosity and permeability, there is no variation in flow in the θ-direction and Z-direction (ignoring gravity segregation). Therefore, the interstitial velocity, V, is a function of the radial distance r,

$$V(r) = \frac{q_o}{2\pi r h \phi} = \frac{V_o r_o}{\phi r} \tag{19}$$

Thus, the velocity has to be updated with each space increment. The dimensionless form for the balance equation is given in appendix A.

6. Numerical Solution Method

The Crank-Nicolson method[29] was used to solve the four simultaneous equations.[12-15] The method is convergent and more stable than the forward and backward difference method.[28] However, numerical dispersion is still a problem, especially for large Pe. The numerical error caused by numerical dispersion is dependent on the numerical increments of time and space, Δx and Δt. For the convection-dispersion equation, it was found that there is no oscillation if $\Delta x < 2L/P_e$.[31] To test the accuracy of the numerical solutions, various time and space increments were tested. In this work, the sizes of the

reduced space increment and the reduced time-step size were chosen to be 0.01 and 0.002, respectively. The finite difference solution for the set of equations is given in appendix B. To verify the numerical method, the CDAC model was tested with the experimental data reported by Coats and Smith,[14] and Baker.[18] Coats and Smith have conducted miscible displacement tests by injecting calcium chloride into sandstone cores and unconsolidated sandpacks to displace sodium chloride. Figure 10 shows the effluent concentration profiles of calcium chloride from two experiments. The fitted parameters for the two tests are also given in the figure. Baker has conducted miscible displacement experiments in a vugular limestone core of a permeability of 5.4 md and a porosity of 11.9%. Xylene was injected into the core of 9.4 cm length to displace benzene at a flow rate of 702 cm^3/sec. Figure 11 shows the effluent concentration profile of xylene and the fitted results. No adsorption was assumed for both cases. A case with dispersion and adsorption was reported by Huang and Novosad.[26] Their data were fitted with the CDA model (eq. 11) as shown in figure 12 with all parameters. So far, no experimental data have been reported for combined effects of three mechanisms: dispersion, adsorption, and capacitance. Coreflooding experiment with consolidate core can provide the data for the study of the combined effects of the three mechanisms.

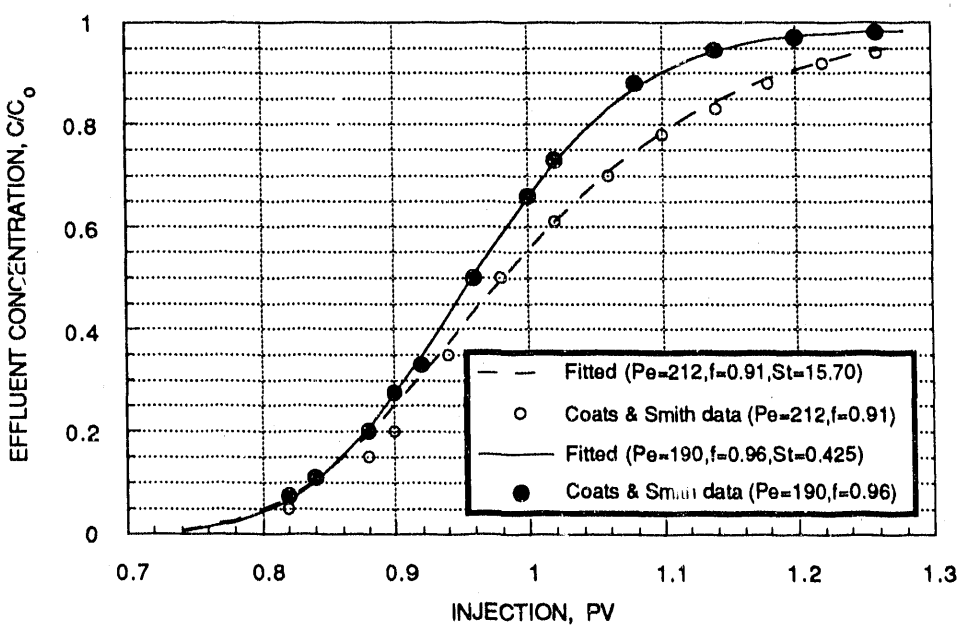

FIGURE 10. - Fitted results for CDC model with Coats and Smith data.[24]

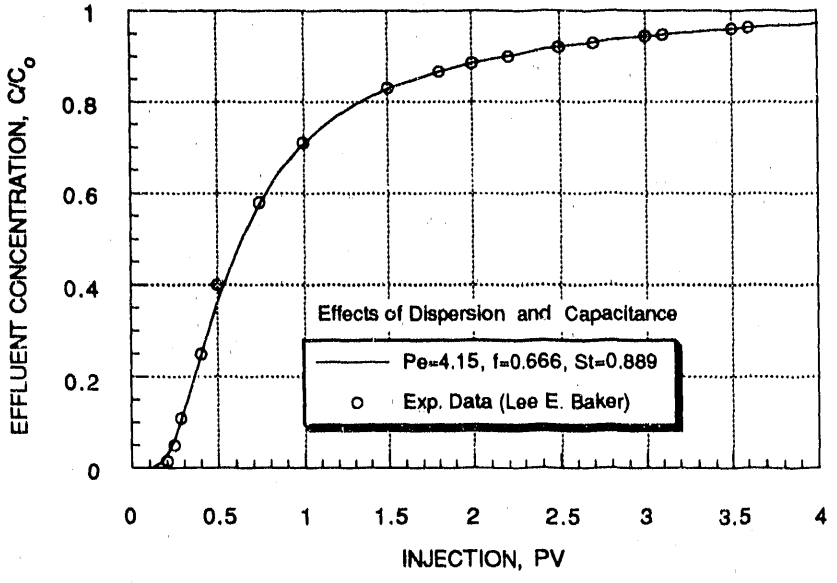

FIGURE 11. - Fitted results for CDC model with Baker data.[28]

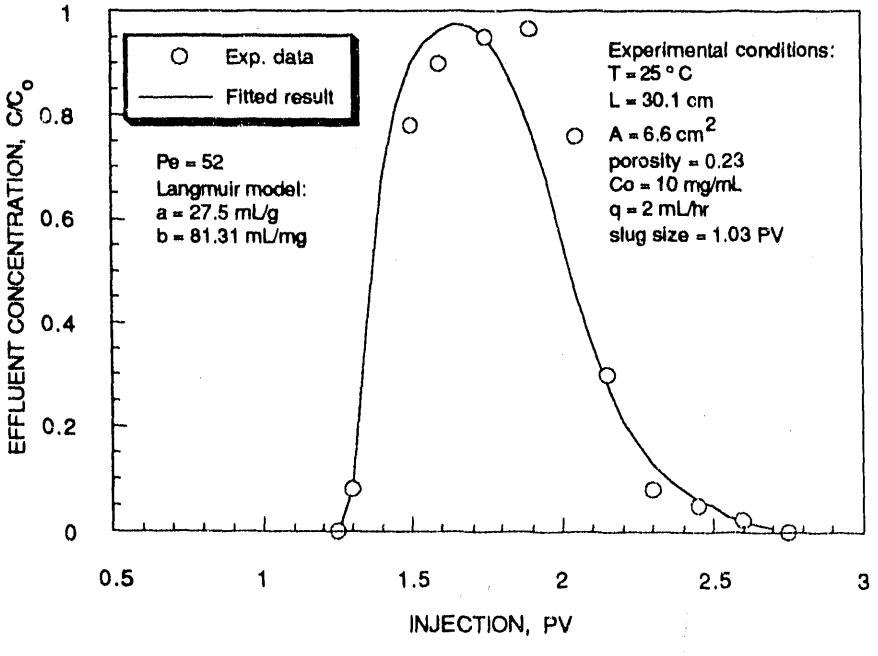

FIGURE 12. - Effluent concentration of surfactant (AOS C1618) through 30-cm-long Berea core[36] and the fitted Langmuir model.

7. Parameter Determination

The parameters in the models were determined by matching the effluent concentration profiles. This procedure is usually carried out by trial-and-error. Several techniques have been developed for automatic history matching which could generate a set of optimized values for the parameters. The methods include a least-squares and linear programming method;[32] an optimal control and gradient optimization method;[33] regression analysis and steepest descent algorithms;[34-35] an error-weighted gradient method;[36] the Gauss-Newton least-squares method;[37] and quadratic programming.[38] Some authors utilized the combination of two or more algorithms.[39-44] Each method has application limitations. Among these methods, the least-squares and linear programming (LSLP) method was tested and applied to this work. No further efforts were made in testing other matching methods in this study.

The basic assumption involved in the LSLP method is a linear relationship between the parameter values and the simulation results. Thus, the quality of the generated optimal parameter values depends on how closely this linear relationship approximates the actual functional dependence between the parameters and simulated results. In the general CDAC model, some of the parameters such as Pe and τ can be determined separately from the tracer 's effluent concentration profile.

To obtain the optimized values for those parameters in the above-mentioned models, several simulation runs are required to match a set of experimental data. Each run has a random set of parameter values. The number of data points (I) should be greater than the number of parameters (J). We set an upper limit x_{ju} and lower limit x_{jl} for each parameter x_j. Thus, $x_{jl} \le x_j \le x_{ju}$. The errors between the calculated values and the experimental data points (ε_i) are assumed to be linearly dependent on the parameters (x_j). Thus, for each data point, we have a linear equation

$$\varepsilon_i = a_{io} + \sum_{j=1}^{J} a_{ij} x_j, \quad i+1,2,\ldots,I \qquad I = \text{number of data points}$$

The coefficients a_{ij} are determined by least squares. Defining the deviation as

$$D_i^r \equiv \varepsilon_i^r - \sum_{j=0}^{J} a_{ij} x_j^r, \quad r=1,2,\ldots,N \qquad N = \text{number of simulation runs}$$

and applying the least-squares technique, i.e.,

$$\sum_{r=1}^{N} (D_i^r)^2 = \min,$$

we can obtain

$$\sum_{j=0}^{J} \left[\sum_{j=0}^{N} x_h^r \, x_j^r \right] a_{ij} = \sum_{j=0}^{N} \varepsilon_i^r \, x_h^r, \quad \begin{matrix} n = 0, J \\ i = 1, I \end{matrix}$$

For any i, the above equation contains J + 1 simultaneous linear equations with J + 1 unknowns, a_{i0}, a_{i1}, a_{iJ}. This system can be solved as

$$\underline{a}_i = [B]^{-1} \underline{C}_i$$

Where [B] is a matrix of coefficients b_{nj}, $[B]^{-1}$ is the inverse of [B], $\underline{C}_i$ is a column vector, so is $\underline{a}_i$.

$$b_{nj} \equiv \sum_{r=1}^{N} x_n^r x_j^r$$

$$C_{in} \equiv \sum_{r=1}^{N} \varepsilon_i^r x_n^r$$

Once a_{ij} are determined, linear programming techniques will be used to calculate the optimal values for x_j.

To determine a set x_j^* that minimized the sum $\sum_{i=1}^{I} w_i|\varepsilon_i|$ subject to constraints on x_j is the classical linear programming problem,[42] i.e.,

$$\sum_{j=1}^{J} a_{ij} x_j + x_{J+i} - x_{J+I+i} = - a_{i0}, \quad i = 1,2,\ldots. I$$

$$x_j \geq x_{jl} \qquad j = 1,2,\ldots. J.$$
$$x_j \leq x_{ju}$$

$$\sum_{i=1}^{I} w_i \, (x_{J+i} + x_{J+I+i}) = \min.$$

The terms wi are weight factors. Computer coding for the LSLP technique has been developed.

8. Influence of Parameters

The effect of the characteristic parameters on the dimensionless concentration profiles and adsorption of the two zones were analyzed using the CDAC model. The influence of the Peclet number is shown in figure 3 from the CD model, and the capacitance effects are shown in figure 4 from the CDC model. Here, emphasis is placed on the effects which have not been previously analyzed. The effect of the kinetic rate of adsorption and desorption is shown in figure 5. Under the same adsorption capacity number (La) and flow number (J), lowering the kinetic adsorption number (E), i.e., lowering the desorption rate relative to the adsorption rate, will retain the chemical inside the porous media, and thus make the concentration profile tailing. The effect of dead-end pore (parameter f) and adsorption on the effluent concentration profile is shown in figure 13.

After all model parameters have been determined from the effluent concentration matching , the model can be used to estimate the surfactant distribution inside the core. Figure 14 shows a case of surfactant distribution inside a 2-ft-long linear core at a specific time. In the radial flow model, the surfactant concentration profile near the wellbore is shown in figure 15. Note that the surfactant concentration drops faster than in the linear flow case. The information about surfactant concentration profiles in reservoir formations is important for the process design of surfactant injection. The CDAC model can provide this information. The model can also be used to study underground water pollution problems and can be extended to other chemical EOR processes such as polymer flooding and alkaline flooding with some modifications. For multiphase flow, we just need to include water saturation in all the balance equations.

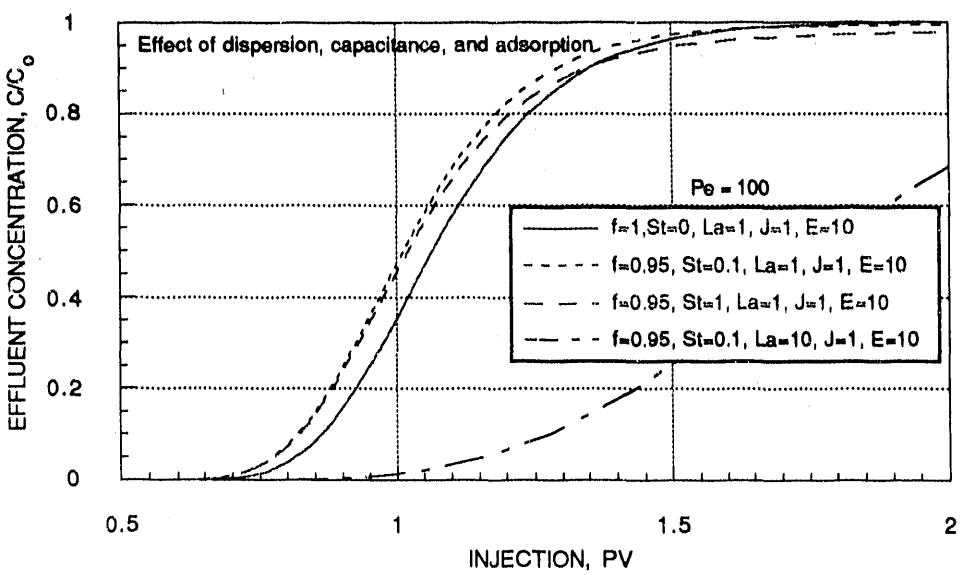

FIGURE 13. - Effects of capacitance dispersion and adsorption on effluent concentration profile.

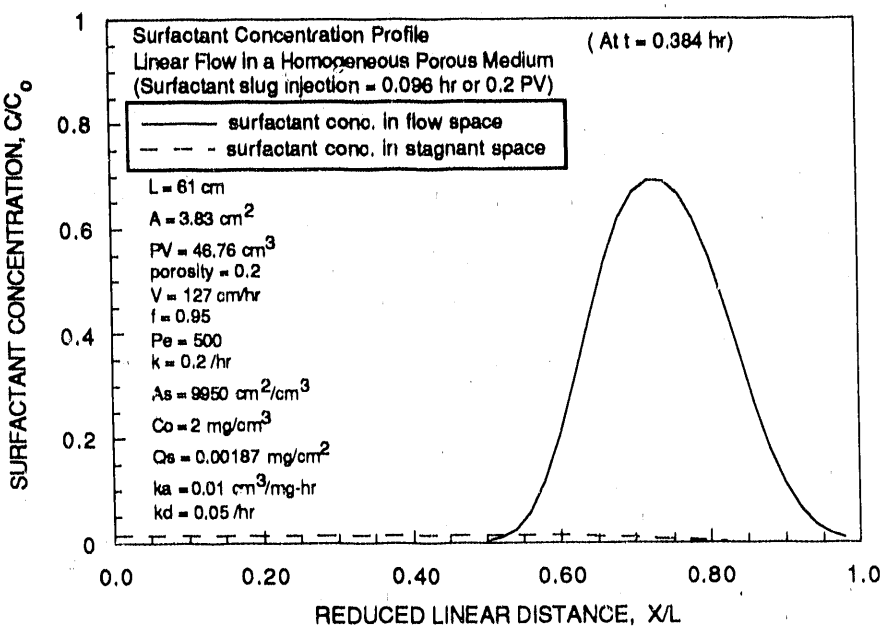

FIGURE 14. - Surfactant concentration profiles in the flowing space and the stagnant space of a 2-ft-long core.

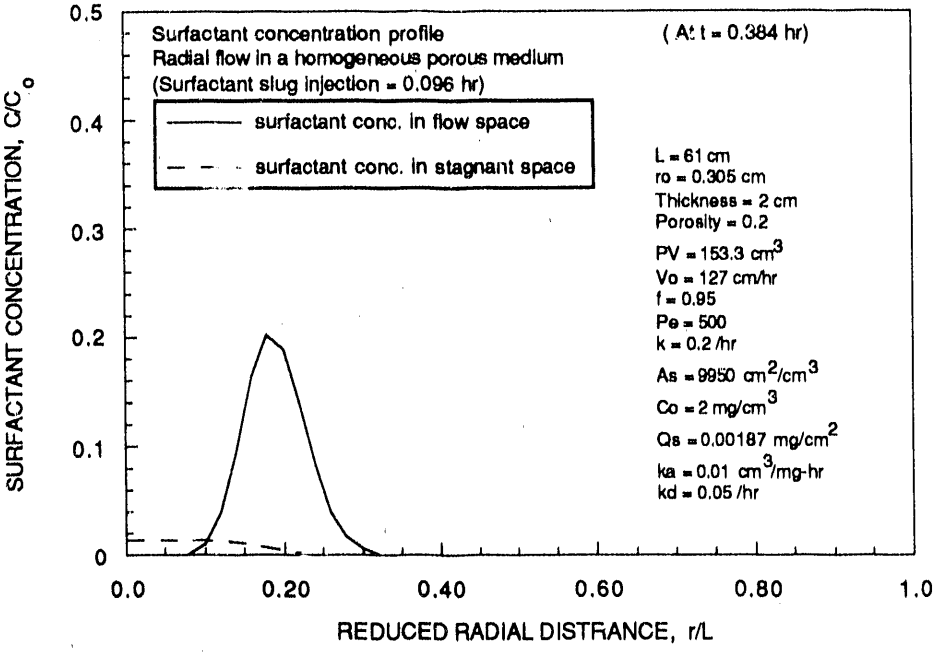

FIGURE 15. - Surfactant concentration profiles in the flowing space and the stagnant space of a 2-ft radius radial-flow core.

EXPERIMENTS

The adsorption of surfactants in reservoir formations is a dynamic process. Trogus et al.,[12] performing experiments with commercial surfactants, observed dynamic adsorption. The amount of surfactant adsorbed depends on the rate of adsorption and the rate of desorption. Flow tests often are used to determine surfactant dynamic adsorption, whereby the surfactant concentration profile is measured at the effluent point using a refractory index (RI) detector or UV detector. This experiment has been used to study the transport of surfactant in porous media. The experiment can be conducted at reservoir conditions with reservoir rock. Accompanying the experimental work, an adequate mathematical model is required to describe the transport and adsorption phenomena of surfactant in porous media. The parameters in the model are determined by matching the effluent surfactant concentration profile. The model will then be used to estimate surfactant concentration distribution inside the porous medium.

1. Experimental Procedure

Dynamic surfactant adsorption tests were conducted in a packed column. The experimental apparatus is shown in figure 16. Stainless steel tubes (1/8-in. ID) of various lengths (1, 2, and 4 ft long) were packed with crushed rocks. The packed column was connected with a sample injection valve (Valco 8-port valve) at the inlet end and with a RI detector at the outlet. The effluent chemical concentration was monitored by a RI detector with a chart recorder. However, the RI detector was not specific in detection of surfactant concentrations because the RI detector also responded to NH_4^+ counter ions resulting from surfactant dissolution and other ions such as Ca^{++} and Na^+ displaced from the sand packing. Therefore, a fraction collector was used to collect sample fractions of the column effluent. These sample fractions were subsequently measured for surfactant concentration by chemical titration or other analysis methods. Before the sample injection, the packed column was evacuated and continuously flushed with deionized water until the column was stable and no peaks for impurities appeared. A specified slug size of sample was injected by switching the sample injection valve to the sample loop for a specific time and then switching back to the water line. Surfactant solutions were injected at constant flow rates of 4 to 10 mL/hr.

Crushed rocks of Berea sandstone, a dolomitic-limestone, and a reservoir sandstone (Liao He reservoir from China) were sieved and measured for specific surface area by the BET method. These sands were chosen to determine if there was a relative difference in surfactant loss due to rock type and surface area.

The apparatus can be used for surfactant adsorption tests at high temperatures and pressures with only minor modifications. Because of limited time, all experiments of this work were conducted at room temperature (75° F) and ambient pressure.

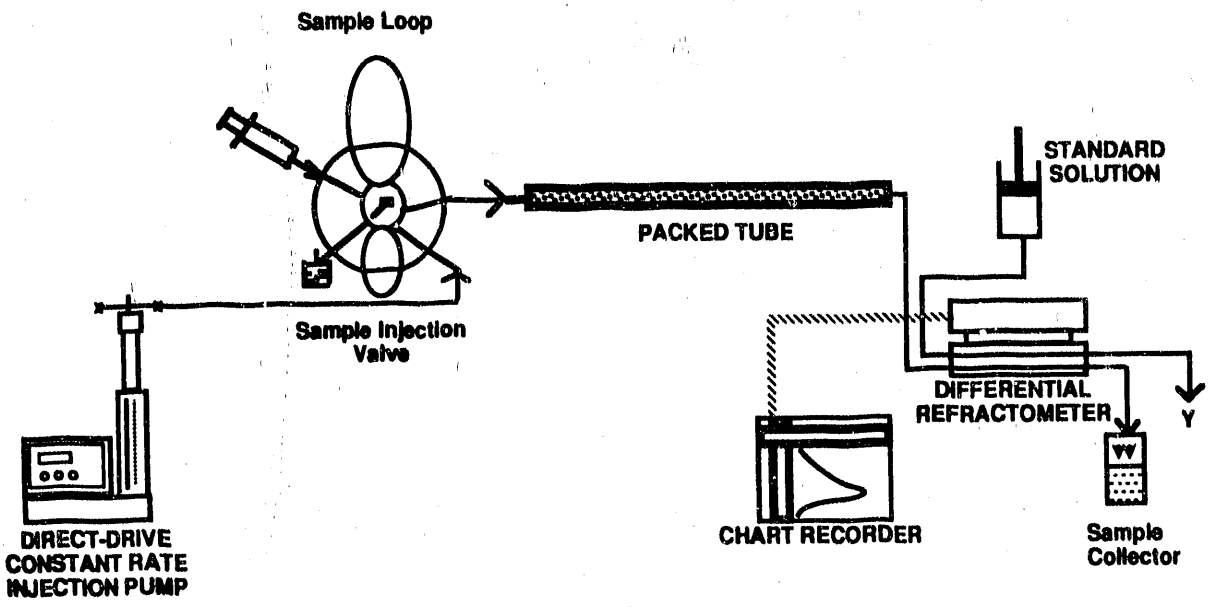

FIGURE 16. - Experimental apparatus.

The transport of surfactant inside a porous medium is governed by many physical aspects: convection flow, dispersion, pore scale diffusion, and adsorption. All these factors will affect the shape of the effluent concentration profile. To identify the effect of adsorption, other fluids, which have negligible adsorption in packed sand, were used as tracers to determine the dispersion and diffusion parameters. The dispersion created at the inlet and outlet of the volume was minimized by shortening the connecting line. The retention time and dispersion caused by the void volume at the inlet and outlet section were also determined and used for calibration.

2. Results and Discussion

Before the experiments for surfactants, dextrose solution (0.2 wt % in DIW) was used to test the effects of capacitance and adsorption. It was assumed that dextrose did not adsorb on Berea sand and that the sandpack column contained no dead-end volume. The effluent concentration profiles are shown in figure 17. The 50% concentration point does appear at the outlet when 1 PV is injected. This verifies the assumption that there is no dead-end volume effect. The effluent concentration profiles are slightly asymetrical. Tailing is partly caused by a small degree of adsorption. Flow experiments were performed for the two nonionic surfactants: 2-(2-butoxyethoxy)ethanol and TRITON X-100. The column was packed with washed Berea sand (80-100 mesh). A 0.5-PV slug of 2-(2-butoxyethoxy)ethanol solution (0.05 wt % in DIW) was injected at a constant flow rate of 7.6 mL/hr to displace DIW from a 2-ft-long packed column. The concentration profile at the outlet is shown in figure 18. The concentration profile

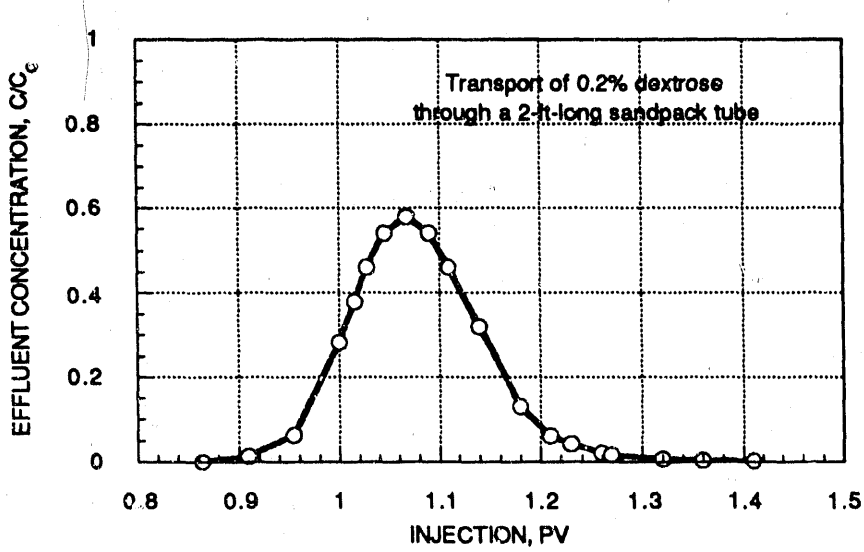

FIGURE 17. - Effluent concentration for dextrose through a 2-ft-long Berea sandpacked column.

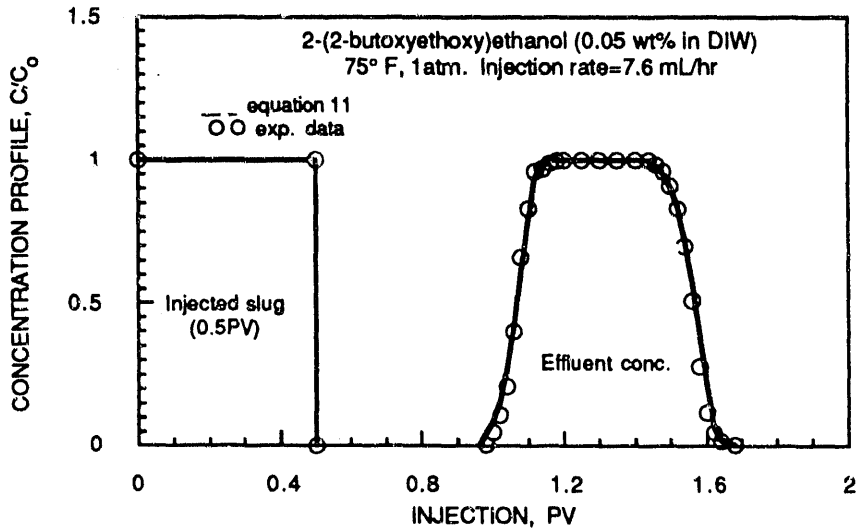

FIGURE 18. - Concentration profiles for the surfactant flowing through a 2-ft-long sandpacked column.

was slightly dispersed and delayed. The result was matched with a Langmuir model of equation 11, described in the above section, and the determined parameters are: $D = 4.7 \times 10^{-4}$ cm^2/sec, $a = 0.015$ cm^3/g-sand, and $b = 0.02$ cm^3/mg. For TRITON X-100, a 1-ft-long column was used because of the strong adsorption. The effluent concentration profile for 1 PV slug injection is shown in figure 19. Compared with that of figure 18, the two concentration profiles are significantly different. The concentration of TRITON X-100 was reduced to less than 10% of the injected concentration after flowing through a 1-ft-long packed column. Obviously, the surfactant was retained on the solid surface strongly, and more than 15 PV of water was required to elute it. The effluent concentration profile has two peaks, which show that two components were separated chromatographically in the column.

A dynamic flow experiment for a dolomitic-limestone packed tube was conducted. The injected surfactant solution was 0.2 wt % of Alipal CD-128 in deionized millipore water. The effluent surfactant concentration measured by RI detector as well as HPLC analysis is shown in figure 20. The HPLC measured surfactant concentration profile was lower than the RI response. The breakthrough curve shows that the 50% concentration appeared at 1.15 PV injection. The delay of the response curve was caused by adsorption. Another flow test was made for Alipal CD-128 solution (0.4 wt % in DIW) on a Berea sandpacked column 2 ft long. The Berea sand was not prewashed, and the average grain surface was about 0.64 m^2/g. The effluent concentration was monitored by RI detector. Also, samples were taken for chemical titration analyses. These results are shown in figure 21, where the chemical titration analyzed concentration closely followed the response of the RI detector except for a small delay in time. The delay was due to the time lag in sampling. However, there was a large discrepancy between the HPLC measured concentration and the concentration measured by chemical analysis. The HPLC analysis indicated a much greater surfactant loss contrasted with the chemical titration method. The discrepancy might be caused by the fine particles from the unwashed Berea sand which were suspended in the solution and carried out by surfactant molecules. Because the fine particles will not pass through the HPLC column, the surfactant adsorbed by the fine particles will not be detected by the HPLC method, but these surfactant molecules will respond in the RI detector and titration analysis.

The retention time of the effluent concentration curve is critical for the adsorption determination. The RI response curve must be corrected by subtracting the retention time due to the void volumes in both inlet and outlet connecting lines. Although using a longer column can mitigate the error, it will increase experimental time and require a large amount of surfactant solution. The design of using a sample injection valve enables one to accurately measure the injection sample size and eliminate the pressure effect on response curve. Before each test run, a slug of the surfactant solution was injected into the system without the packed column to obtain the reference response peak which corresponds to the original solution concentration C_O, and to measure the retention time caused by the void volume.

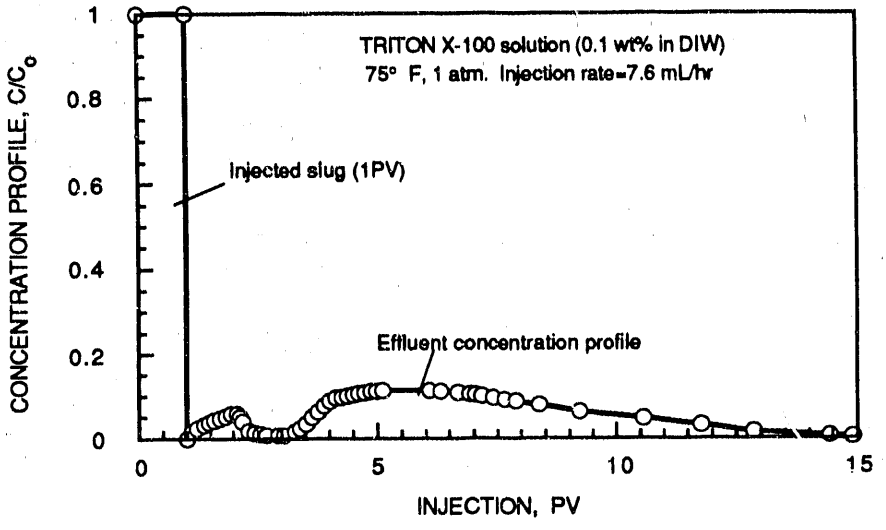

FIGURE 19. - Concentration profiles for the surfactant flowing through a 1-ft-long sandpacked column.

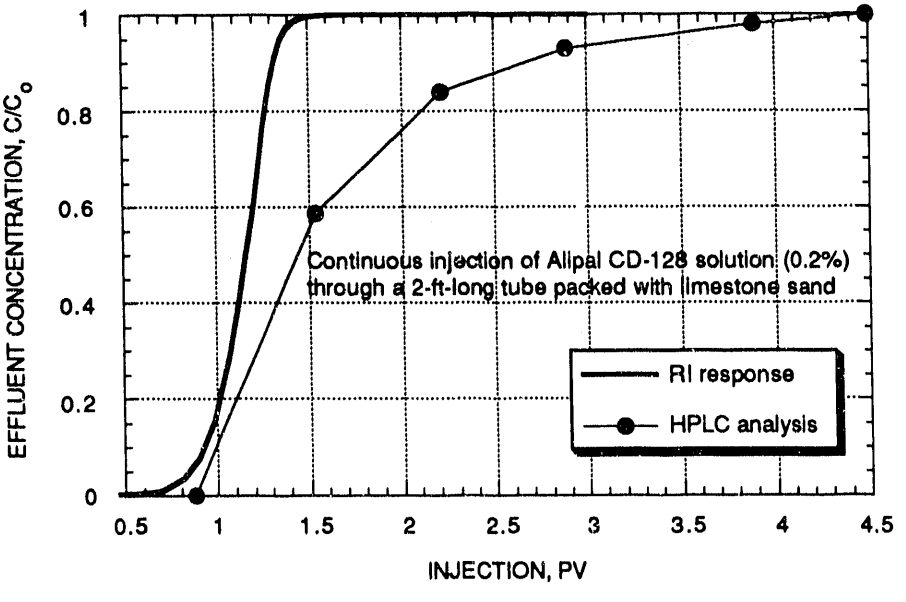

FIGURE 20. - Effluent Alipal CD-128 concentration profile during continuous injection.

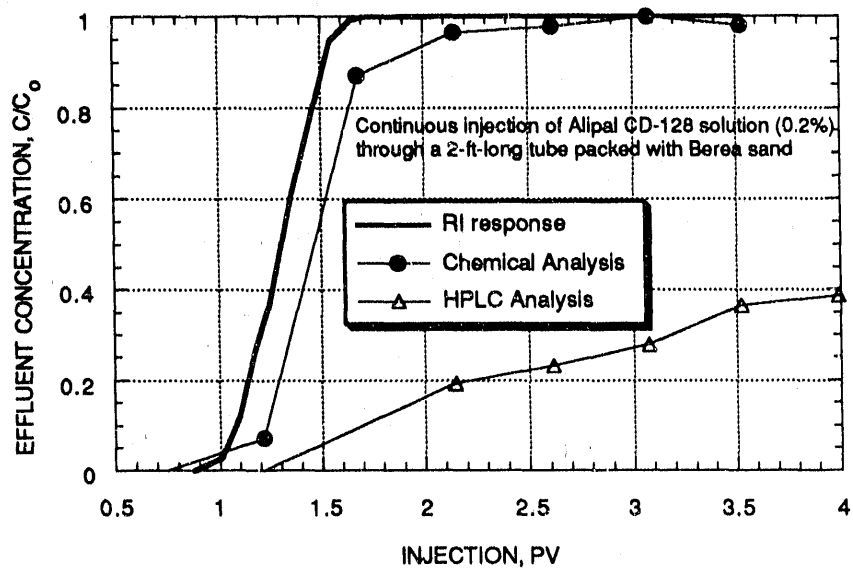

FIGURE 21. - Results of Alipal CD-128 effluent concentration from different analysis methods during continuous injection.

SUMMARY AND CONCLUSIONS

1. Mathematical models and computer codings for surfactant transport and adsorption in linear core and in radial-flow core were developed. Effects of dispersion, adsorption, and capacitance were studied using the developed models.

2. A flow experimental method to study the transport and dynamic sorption of surfactants in sandpack columns was developed. The adsorption and desorption rate constants can be estimated by matching the effluent concentration profile with a suitable mathematical model.

3. The effects of dispersion, adsorption, and capacitance on the effluent concentration profile are not independent. To determine each of these parameters, the effect of each parameter must be identified. A tracer test method can be used to determine the dispersion and capacitance parameters before surfactant injection.

4. The accuracy of the measured retention time of the breakthrough curve is critical to the determination of the capacitance and adsorption-desorption parameters. A longer sandpacked column would be more accurate in the retention time measurements.

5. The radial flow model shows that the surfactant concentration drops sharply near the injection wellbore, which poses the question of whether foam can be generated at a distance far away from the wellbore.

6. From the results of dynamic sorption tests, the adsorption rate of TRITON X-100 is much greater than the desorption rate, and the adsorptions of Alipal CD-128 in Berea sands and limestone are not significant.

7. There is a discrepancy among the measured effluent surfactant concentration using different analysis methods. The HPLC analysis method may not to be good for certain surfactant analysis. Further research is needed to clarify and understand the reason for this discrepancy between the HPLC analysis and the chemical (hyamine) titration.

REFERENCES

1. Falls, A. H., P. A. Gauglitz, G. J. Hirasaki, D. D. Miller, T. W. Patsek, and J. Ratulowski. Development of a Mechanistic Foam Simulator: The Population Balance and Generation by Anap-Off. Pres. at SPE/DOE Sym. on EOR, Tulsa, OK, Apr. 20-23, 1986. SPE/DOE paper 14961.

2. Friedman, F., W. H. Chen, and P. A. Gauglitz. Experimental and Simulation Study of High-Temperature Foam Displacement in Porous Media. Pres. at SPE/DOE Sym. on EOR, Tulsa, OK, Apr. 17-20, 1988. SPE/DOE paper 17357.

3. Hirasaki, G.J., and J.B. Lawson. Mechanisms of Foam Flow in Porous Media: Apparent Viscosity in Smooth Capillaries. Soc. Pet. Eng. J., April 1985, pp.176-190.

4. Llave, F. M., T. H. Chung, R. W. Louvier, and D. A. Hudgins. Gas Miscible Displacement: Foams for Mobility Control and Improvement in Gas Sweep Efficiency. Dept. of Energy Report No. NIPER-431, Dec. 1989.

5. Scamehorn, J. F., R. S. Schechter, and W. H. Wade. Adsorption of Surfactants on Mineral Oxide Surfaces From Aqueous Solutions; I:Isomerically Pure Anionic Surfactants; II; Binary Mixtures of Anionic Surfactants; III: Binary Mixtures of Anionic and Nonionic Surfactants. J. Colloid Interface Sci., v. 85, No. 2, Feb. 1982, pp. 463-501.

6. Somasundaran, P. and G. E. Agar. The Zero Point Charge of Calaite. J. Colloid Interface Sci. v. 24, 1967, pp. 433-445.

7. Al-Hashim, H. S., M. S. Celik, M. M. Oskay, and H. Y. Al-Yousef. Adsorption and Precipitation Behavior of Petroleum Sulfonates from Saudi Arabian Limestone. J. Pet. Sci. Eng., v. 1, 1988, pp. 335-344.

8. Ross, S. R. and J. P. Olivier. On Physical Adsorption. Interscience, New York, 1964.

9. Hsu, C. C., B. W. Wojciechowski, W. Rudzinski, and J. Narkiewicz. An Improved Method for Evaluating Surface Heterogeneity for Various Models of Local Adsorption. J. Colloid Interface Sci., v. 67, No. 2, Nov. 1978, pp. 292-303.

10. Avnir, D., D. Farin, and P. Pfeifer. Surface Geometric Irregularity of Particulate Materials: The Fractal. J. Colloid Interface Sci., v. 103, No. 1, Jan. 1985, pp. 112-123.

11. Somasundaran, P. Adsorption from Flooding Solutions in Porous Media: A Study of Interactions of Surfactants and Polymers with Reservoir Minerals. Dept. of Energy Report No. DOE/BC/10848-5, April 1987.

12. Trogus, F., T. Sophany, R. S. Schechter, and W. H. Wade. Static and Dynamic Adsorption of Anionic and Nonanionic Surfactants. Soc. Pet. Eng. J., Oct. 1977, pp. 337-344.

13. Huang, A. H. The Surface Excess Concept in Modeling Surfactant Adsorption in Porous Media. M.S. Thesis, University of Calgary, 1985.

14. Coats, K. H. and B. D. Smith. Dead-End Pore Volume and Dispersion in Porous Media. Soc. Pet. Eng. J., March 1964, pp. 73-84.

15. Ramirez, W. F., P. J. Shuler, and F. Friedman. Convection, Dispersion, and Adsorption of Surfactants in Porous Media. Soc. Pet. Eng. J., Dec. 1980, pp. 430-438.

16. Aris , R. and N. R. Amundson. Some Remarks on Longitudinal Mixing or Diffusion in Six Beds. AIChE J., v. 3, 1957, pp. 280-282.

17. Perkins, T. K. and O. C. Jonston. A Review of Diffusion and Dispersion in Porous Media. Soc. Pet. Eng. J., March 1963, pp. 70-84.

18. Baker, L. E. Effects of Dispersion and Dead-End Pore Volume in Miscible Flooding. Soc. Pet. Eng. J., June 1977, pp. 219-227.

19. Blackwell, R. J. Laboratory Studies of Microscopic Dispersion Phenomena. Soc. Pet. Eng. J., March 1962, p. 1-8.

20. Deans, H. A. A Mathematical Model for Dispersion in the Direction of Flow in Porous Media. Soc. Pet. Eng. J., v. 3, 1963, pp. 49-52.

21. Baticky, J. P., B. B. Maini, and D. B. Fisher. Simulation of Miscible Displacement in Full-Diameter Carbonate Cores. Soc. Pet. Eng. J., v. 22, 1982, pp-647-657.

22. Heller, J. P. and J. J. Taber. Improvement of CO_2 Flood Performance, Annual Report. Dept. of Energy Report No. DOE/MC/21136-6, June 1986, p. 77.

23. Danckwerts, P. V. Continuous Flow Systems, Distribution of Residence Times. Chem. Eng. Sci. v. 2, No. 1, 1953, pp. 1-13.

24. Jasti, J. K., R. N. Vaidya, and H. S. Fogler. Capacitance Effects in Porous Media. Pres. at SPE Annual Tech. Conf. and Exhib., Dallas, TX, Sept. 27-30, 1987. SPE paper 16707.

25. Salter, S. J. and K. K. Mohanty. Multiphase Flow in Porous Media: I. Macroscopic Observations and Modeling, and II. Pore-Level Modeling. Pres. at SPE Annual Tech. Conf. and Exhib., New Orleans, LA, Sept. 26-29, 1982. SPE papers 11017 and 11018.

26. Huang, A. Y. and J. J. Novosad. Modeling of Adsorption of Foam-Forming Surfactants in Porous Media in Fundamentals of Adsorption. Proc., 2nd Eng. Foundation Conf., Santa Barbara, CA, May 4-9, 1986.

27. Satter, A, Y. M. Shum, W. T. Adams, and L. A. Davis. Chemical Transport in Porous Media with Dispersion and Rate-Controlled Adsorption. Soc. Pet. Eng. J., June 1980, pp. 129-138

28. Barakat, H. Z. and J. A. Clark. On the Solution of the Diffusion Equations by Numerical Methods. J. Heat Transfer, v. 88, No. 4, Nov. 1966, pp. 421-427.

29. Von Rosenberg, D. U. Methods for Numerical Solution of Partial Differential Equations. American Elsevier Publishing Co. Inc., New York, 1969.

30. Bidner, M. S. and V. C. Vampa. A General Model for Convection-Dispersion-Dynamic Adsorption in Porous Media with Stagnant Volume. J. Pet. Sci. Eng., v. 3, 1989, pp. 267-281.

31. Price, H. S., R. S. Varga, and J. E. Warren. Application of Oscillation Matrices to Diffusion-Convection Equations. J. Math. Phys., v. 45, 1966, pp. 301-311.

32. Coats, K. H., J. R. Dempsey, and J. H. Henderson. A New Technique for Determining Reservoir Description from Field Performance Data. Soc. Pet. Eng. J., March 1970, pp. 66-74.

33. Chen, W. H., G. R. Gavalas, J. H. Seinfeld, and M. L. Wasserman. A New Algorithm for Automatic History Matching. Soc. Pet. Eng. J., Dec. 1974, pp. 593-608.

34. Jacquard, P, and C. Jain. Permeability Distributions from Field Pressure Data. Soc. Pet. Eng. J., Dec. 1965, pp-281-293.

35. Jahns, H. O.. A Rapid Method for Obtaining a Two-Dimensional Reservoir Description from Well Pressure Response Data. Soc. Pet. Eng. J., Dec. 1966, pp. 315-327.

36. Slater, G. E., and E. J. Durrer. Adjustment of Reservoir Simulation Models to Match Field Performance. Soc. Pet. Eng. J., Sept. 1971, pp. 295-305.

37. Thomas, L. K., L. J. Hellums, and G. M. Reheis. A Nonlinear Automatic History Matching Technique for Reservoir Simulation Models. Soc. Pet. Eng. J., Dec. 1972, pp. 508-514.

38. Yeh, W. W. Optimal Identification of Parameters in an Inhomogeneous Medium with Quadratic Programming. Soc. Pet. Eng. J., Oct. 1975, pp. 371-375.

39. Carter, R. D., L. F. Kemp Jr., A. C. Pierce, and D. L. Williams. Performance Matching with Constants. Soc. Pet. Eng. J., April 1974, pp. 187-196.

40. Chavent, C., M. Dupuy, and P. Lemonnier. History Matching by Use of Optimal Control Theory. Soc. Pet. Eng. J., Feb. 1975, pp. 74-86.

41. Hirasaki, G. J. Sensitivity Coefficients for History Matching Processes. Soc. Pet. Eng. J., Feb. 1975, pp. 39-49.

42. Shah, P. C., G. R. Gavalas, and J. H. Seinfeld. Error Analysis in History Matching: The Optimum Level of Parameterization. Soc. Pet. Eng. J., June 1978, pp. 219-228.

43. Watson, A. T. and W. J. Lee. A New Algorithm for Automatic History Matching Production Data. Pres. at SPE Unconventional Gas Tech. Sym., Louisville, KY, May 16-21, 1986. SPE paper 15228.

44. Yang, P-H., R. V. Armasu, and A. T. Watson. Automatic History Matching with Variable-Metric Methods. Proc., SPE Annual Tech. Conf. and Exhib., Dallas, TX, 1987, pp. 27-30. SPE paper 16977.

45. Somasundaran, P., and D. W. Fuerstenau. Mechanisms of Alkyl Sulfonate Adsorption at the Alumina-Water Interface. J. Phys. Chem., v. 70, No. 1, Jan. 1966.

46. Dick, S. G., D. W. Fuerstenau, and T. W. Healy. Adsorption of Alkylbenzene Sulfonate (ABS) Surfactants at the Alumina-Water Interface. J. Colloid Interface Sci., v. 37, No. 3, Nov. 1971, pp. 595-602.

47. Fuerstenau, D. W., and T. Wakamatsu. Effect of pH on the Adsorption of Sodium Dodecane-Sulphonate at the Alumina/Water Interface. Faraday Discussion, Chem. Soc., v. 59, 1976, p. 157.

48. Tamamushi, B. and K. Tamaki. Adsorption of Long-Chain Electrolytes at the Solid/Liquid Interface. Trans. Faraday Soc., v. 55, 1959, pp. 1007-1012.

49. French, T. R. and T. E. Burchfield. Design and Optimization of Alkaline Flooding Formulations. Pres. at SPE/DOE Sym. on EOR, Tulsa, OK, Apr. 22-25, 1990. SPE/DOE paper 20238.

APPENDIX A

DIMENSIONLESS EQUATIONS AND CHARACTERISTIC PARAMETERS

A. General Convection-Dispersion-Adsorption-Capacitance (CDAC) Model

Dimensionless variables:

$$\eta = \frac{x}{L},\ \tau = \frac{Vt}{L},\ Y = \frac{C}{C_o},\ Y^* = \frac{C^*}{C_o},\ Y_s = \frac{C_s}{Q_s},\ Y_s^* = \frac{C_s^*}{Q_s},$$

Dimensionless parameters:

$P_e = \frac{VL}{D}$, Peclet Number

$S_t = \frac{kL}{V}$, Stanton Number

$L_a = \frac{A_s Q_s}{\phi C_o}$, Adsorption Capacity Number

$E = \frac{k_d}{k_a C_o}$, Kinetic Adsorption Number

$J = \frac{V}{L k_a C_o}$, Flow Rate Number

Equations 12, 13, 14, and 15 become

$$\frac{1}{P_e}\frac{\partial^2 Y}{\partial \eta^2} - \frac{\partial Y}{\partial \eta} = f\left[\frac{\partial Y}{\partial \tau} + L_a \frac{\partial Y_s}{\partial \tau}\right] + (1-f)\left[\frac{\partial Y^*}{\partial \tau} + L_a \frac{\partial Y_s^*}{\partial \tau}\right] \tag{A-1}$$

$$\left[\frac{\partial Y^*}{\partial \tau} + L_a \frac{\partial Y_s^*}{\partial \tau}\right] = S_t\left(Y - Y^*\right) \tag{A-2}$$

$$\frac{\partial Y_s}{\partial \tau} = \frac{1}{J}\left[Y(1 - Y_s) - E\,Y_s\right] \tag{A-3}$$

$$\frac{\partial Y_s^*}{\partial \tau} = \frac{1}{J}\left[Y^*\left(1 - Y_s^*\right) - E\,Y_s^*\right] \tag{A-4}$$

The boundary conditions are

$$Y(\tau, 0) - \frac{1}{P_e}\frac{\partial Y}{\partial \eta}\Big|_{\eta=1} \begin{array}{ll} = 1, & 0<\tau<\tau_1 \\ = 0, & \tau>\tau_1 \end{array} \tag{A-5}$$

$$\frac{\partial Y}{\partial \eta}\Big|_{\eta=1} = 0 \tag{A-6}$$

B. Convection-Dispersion-Adsorption (CDA) Model

When f = 1, (thus, Y* and Ys* disappear), the CDAC model reduces to the CDA model, and equations A-1 to A-4 reduce to

$$\frac{1}{P_e}\frac{\partial^2 Y}{\partial \eta^2} - \frac{\partial Y}{\partial \eta} = \frac{\partial Y}{\partial \tau} + L_a \frac{\partial Y_s}{\partial \tau} \tag{A-7}$$

$$\frac{\partial Y_s}{\partial \tau} = \frac{1}{J}\left[Y(1 - Y_s) - EY_s\right] \tag{A-8}$$

Equations A-7 and A-8 are the dimensionless forms of equations 9 and 10.

For the case that adsorption reaches equilibrium instantaneously, equations A-7 and A-8 reduce to

$$\frac{1}{P_e}\frac{\partial^2 Y}{\partial \eta^2} - \frac{\partial Y}{\partial \eta} = \left[1 + \frac{L_a E}{(E+Y)^2}\right]\frac{\partial Y}{\partial \tau} \tag{A-9}$$

which is the dimensionless form of equation 11.

C. Convection-Dispersion-Capacitance (CDC) Model

When there is no adsorption, i.e., $L_a = 0$, the CDAC model reduces to the CDC model, and equations A-1 to A-4 reduce to

$$\frac{1}{P_e}\frac{\partial^2 Y}{\partial \eta^2} - \frac{\partial Y}{\partial \eta} = f\frac{\partial Y}{\partial \tau} + (1 - f)\frac{\partial Y^*}{\partial \tau} \tag{A-10}$$

$$\frac{\partial Y^*}{\partial \tau} = S_t\left(Y - Y^*\right) \tag{A-11}$$

Equations A-10 and A-11 are the dimensionless forms of equations 3 and 4.

D. Convection-Dispersion (CD) Model

When f = 1 and La = 0, i.e., no adsorption and capacitance effects, equations A-1 to A-4 reduce to

$$\frac{1}{P_e}\frac{\partial^2 Y}{\partial \eta^2} - \frac{\partial Y}{\partial \eta} = \frac{\partial Y}{\partial \tau} \tag{A-12}$$

which is the dimensionless form for the CD model, equation 1.

E. Radial Flow Model

Dimensionless variables:

$$\eta = \frac{x}{L} = \frac{r - r_o}{R - r_o},\ \eta_o = \frac{r_o}{L},\ \tau = \frac{V_o t}{L},\ Y^* = \frac{C^*}{C_o},\ Y_s = \frac{C_s}{Q_s},\ Y_s^* = \frac{C_s^*}{Q_s}$$

Dimensionless parameters:

$$P_e = \frac{V_o L}{D}$$

$$S^* = \frac{KL}{V_o}$$

$$L_a = \frac{A_s Q_s}{\phi C_o}$$

$$E = \frac{K_d}{K_a C_o}$$

$$J = \frac{V_o}{L \cdot k_a \cdot C_o}$$

Equation 16 becomes

$$\frac{1}{P_e}\frac{\partial^2 Y}{\partial \eta^2} + \left(\frac{1}{P_e} - \frac{\eta_o}{\phi}\right) \cdot \frac{1}{\eta + \eta_o}\frac{\partial Y}{\partial \eta} = f\left[\frac{\partial Y}{\partial \tau} + L_a \frac{\partial Y_s}{\partial \tau}\right] + (1 - f)\left[\frac{\partial Y^*}{\partial \tau} + L_a \frac{\partial Y_s^*}{\partial \tau}\right]$$

APPENDIX B

NUMERICAL SOLUTION FOR THE CDAC MODEL

1. Crank-Nicolson finite difference method

$$\frac{\partial^2 Y}{\partial \eta^2} = \frac{1}{2h^2}\left(Y_{i+1}^{n} - 2Y_i^{n} + Y_{i-1}^{n} + Y_{i+1}^{n+1} - 2Y_i^{n+1} + Y_{i-1}^{n+1}\right) \tag{B-1}$$

$$\frac{\partial Y}{\partial \eta} = \frac{1}{4h}\left(Y_{i+1}^{n} - Y_{i-1}^{n} + Y_{i+1}^{n+1} - Y_{i-1}^{n+1}\right) \tag{B-2}$$

$$\frac{\partial Y}{\partial \eta} = \frac{1}{\theta}\left(Y_i^{n+1} - Y_i^{n}\right) \tag{B-3}$$

$$Y = \frac{1}{2}\left(Y_i^{n+1} + Y_i^{n}\right) \tag{B-4}$$

2. The finite difference expression for equation A-1 is

$$-\left(\frac{1}{4h} + \frac{1}{2h^2 P_e}\right) Y_i^{n+1} + \left[\frac{f}{\theta} + \frac{1}{h^2 P_e} + \frac{(1-f)S_t}{2} + \frac{L_a f}{2J}\left(1 - Y_{si}^{n+1/2}\right)\right] Y_i^{n+1}$$

$$+\left(\frac{1}{4h} - \frac{1}{2h^2 P_e}\right) Y_{i+1}^{n+1} = \left(\frac{1}{4h} + \frac{1}{2h^2 P_e}\right) Y_{i-1}^{n} + \left[\frac{f}{\theta} - \frac{1}{h^2 P_e} - \frac{(1-f)S_t}{2} - \frac{L_a f}{2J}\left(1 - Y_{si}^{n+1/2}\right)\right]$$

$$Y_i^{n} - \left(\frac{1}{4h} - \frac{1}{2h^2 P_e}\right) Y_{i+1}^{n} + (1-f) S_t Y_i^{*n+1/2} + \frac{L_a f E}{J} Y_{si}^{n+1/2} \tag{B-5}$$

The variables Y^* and Y_s at time step n+1/2 were used to solve equation B-5. Taylor expansions truncated after the second term were employed to obtain the values of $Y^{*n+1/2}$ and $Y_s^{n+1/2}$. Time derivatives were obtained from equations A-2 and A-4.

$$Y_i^{*n+1/2} = Y_i^{*n} + \frac{\theta}{2}\left\{S_t\left(Y_i^{n} - Y_i^{*n}\right) - \frac{L_a}{J}\left[Y_i^{*n}\left(1 - Y_{si}^{*n}\right) - E Y_{si}^{*n}\right]\right\} \tag{B-6}$$

$$Y_{si}^{n+1/2} = Y_{si}^{n} + \frac{\theta}{2J}\left[Y_i^{n}\left(1 - Y_{si}^{n}\right) - E Y_{si}^{n}\right] \tag{B-7}$$

At the inlet boundary (i=1)

$$\left[\frac{f}{\theta} + \frac{P_e}{2} + \frac{1}{h} + \frac{1}{h^2 P_e} + \frac{(1-f)S_t}{2} + \frac{L_a f}{2J}\left(1 - Y_{si}^{n+1/2}\right)\right] Y_1^{n+1} - \frac{1}{h^2 P_e} Y_2^{n+1}$$

$$= \left[\frac{f}{\theta} - \frac{P_e}{2} - \frac{1}{h} - \frac{1}{h^2 P_e} - \frac{(1-f)S_t}{2} - \frac{L_a f}{2J}\left(1 - Y_{si}^{n+1/2}\right)\right] Y_1^{n} + \frac{1}{h^2 P_e} Y_2^{n} \tag{B-8}$$

$$+(1-f)\,S_t\,Y_1^{*n+1/2} + \frac{L_a\,fE}{J}\,Y_{s1}^{n+1/2} + \left(P_e + \frac{2}{h}\right)U$$

At the outlet boundary (l=R+1)

$$-\frac{1}{h^2 P_e}\,Y_R^{n+1} + \left[\frac{f}{\theta} + \frac{1}{h^2 P_e} + \frac{(1-f)\,S_t}{2} + \frac{fL_a}{2J}\left(1 - Y_{sR+1}^{n+1/2}\right)\right] Y_{R+1}^{n+1}$$

$$= \frac{1}{h^2 P_e}\,Y_R^{n} + \left[\frac{f}{\theta} - \frac{1}{h^2 P_e} - \frac{(1-f)\,S_t}{2} - \frac{fL_a}{2J}\left(1 - Y_{sR+1}^{n+1/2}\right)\right] Y_{R+1}^{n} + (1-f)\,S_t\,Y_{R+1}^{*n+1/2}$$

$$+\frac{fL_aE}{2J}\,Y_{sR+1}^{n+1/2}$$

3. Y_{sl}^{n+1} was obtained from equation A-3

$$\left(1 + \frac{\theta\left(Y_l^{n+1} + Y_l^{n}\right)}{4J} + \frac{\theta E}{2J}\right) Y_{sl}^{n+1} = \left(1 - \frac{\theta\left(Y_l^{n+1} + Y_l^{n}\right)}{4J} + \frac{\theta E}{2J}\right) Y_{sl}^{n} + \frac{\theta\left(Y_l^{n+1} + Y_l^{n}\right)}{2J}$$

4. For the values of Y_{sl}^{*n+1} and Y_l^{*n+1}, iteration method is needed to solve the following two equations from A-4 and A-2

$$\left(1 + \frac{\theta\left(Y_l^{*n+1} + Y_l^{*n}\right)}{4J} + \frac{\theta E}{2J}\right) Y_{sl}^{*n+1} = \left(1 - \frac{\theta\left(Y_l^{*n+1} + Y_l^{*n}\right)}{4J} + \frac{\theta E}{2J}\right) Y_{sl}^{*n} + \frac{\theta\left(Y_l^{*n+1} + Y_l^{*n}\right)}{2J}$$

$$\left(1 + \frac{\theta S_t}{2}\right) Y_l^{*n+1} = \left(1 - \frac{\theta S_t}{2}\right) Y_l^{*n} + \frac{\theta S_t}{2}\left(Y_l^{n+1} + Y_l^{n}\right) - L_a\left(Y_{sl}^{*n+1} + Y_{sl}^{*n}\right)$$

APPENDIX C

BATCH EXPERIMENTAL RESULTS

Equilibrium adsorption isotherms for Alipal CD-128 surfactants on Berea sand were determined at 75° F. Surfactant concentrations in deionized water range from 10 to 1,000,000 μ-mol/L. Results are shown in figure C-1. The adsorption isotherm shows several regions. At low concentrations, the adsorption of surfactant increased slightly with surfactant concentration. At higher concentrations, the adsorption increased rapidly with surfactant concentration and then reached a plateau at surfactant concentrations higher than about 10,000 μ mol/L. This behavior is similar to the adsorption of surfactant on pure mineral oxides (fig. 2). Because the total surface area for each sand sample may not be the same (sand grain size from 80 to 100 mesh), the measured data had greater scatter.

The losses of Alipal CD-128 on limestone, kaolinite, and Berea sandstone were compared on a surface-area basis (fig. C-2). The surfactant loss data were measured by equilibrium tests and chemical analysis using the hyamine titration method. The loss of the surfactant due to adsorption and precipitation on limestone was much higher than that on Berea sandstone and kaolinite. Adsorption appears to be only one of several mechanisms that contributed to high surfactant loss. Limestone is largely calcite and will dissolve in water to produce Ca^{++}, CO_3^{--}, HCO_3^-, H_2CO_3, H^+, OH^-, $CaOH^+$, $Ca(OH)_2$. Interaction of these ions with the anionic surfactants can produce precipitation.[6-7]

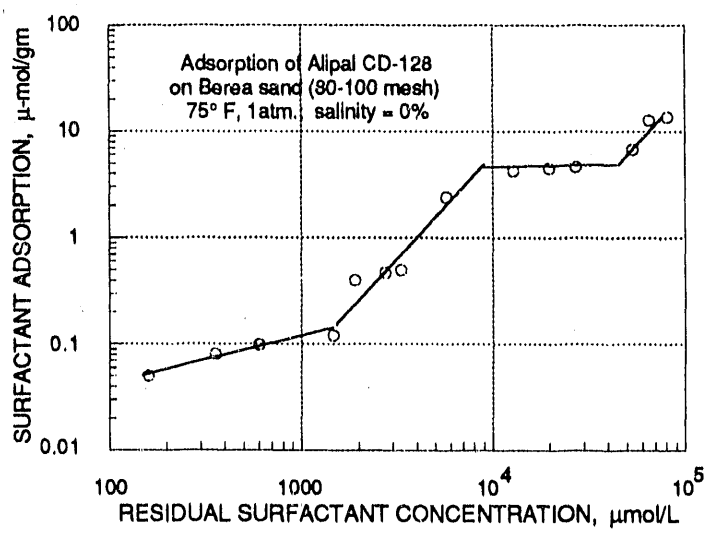

FIGURE C-1. - Adsorption isotherm for Alipal CD-128 on Berea sand.

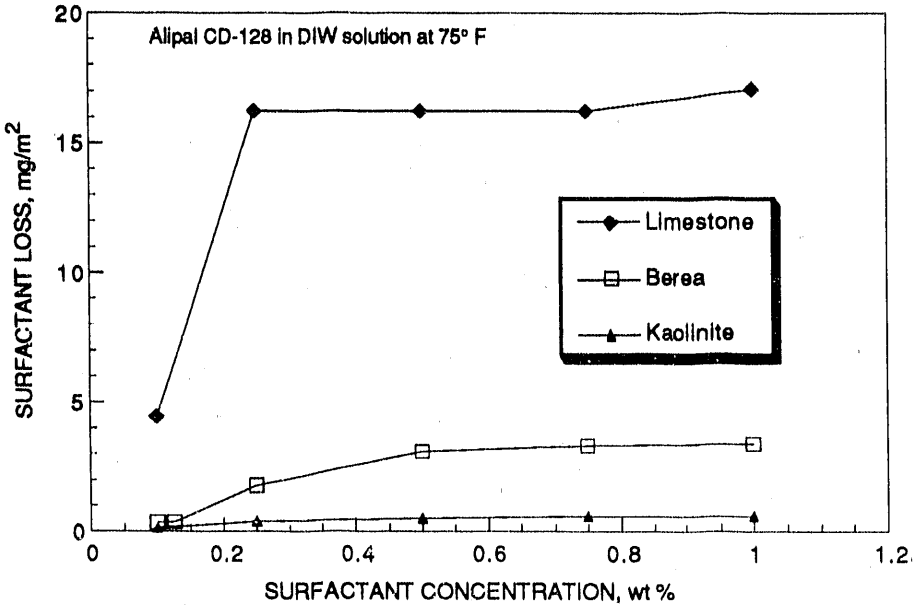

FIGURE C-2. - Alipal CD-128 loss on various media as a function of surface area.

The effects of pH, alkalinity, salinity, alcohol, and temperature on surfactant adsorption were tested for Alipal CD-128 on kaolinite. The pH was measured for mixtures of deionized water (DIW) and various materials used in this work. Results are given as follows:

Material	pH
DIW + washed Berea.....	6.66
DIW + unwashed Berea....	8.33
DIW + kaolinite.....	4.16
DIW + limestone.....	8.88

There was no significant change of the pH-value for the DIW after adding Alipal CD-128. The effect of pH on the adsorption of Alipal CD-128 is shown in figure C-3. The pH-values were adjusted by adding acid (HCl) or base (NaOH) into the solution. It can be seen that the adsorption of Alipal CD-128 is higher at low pH than at high pH values. Many studies have concluded that at constant monomer concentration, the adsorption of anionic surfactants on mineral oxides increases with decreasing pH, because of the increased electrostatic attraction between adsorbate and surface.[5,45-48] With low-pH alkaline agents such as sodium bicarbonate ($NaHCO_3$), surfactant adsorption is reduced significantly, as shown in figure C-4, and may be one of the beneficial aspects of surfactant alkaline flooding.[49] Because of the reduction of surfactant adsorption in the presence of alkaline agents, the surfactant-alkaline injection method facilitates the use of low concentrations of surfactants.

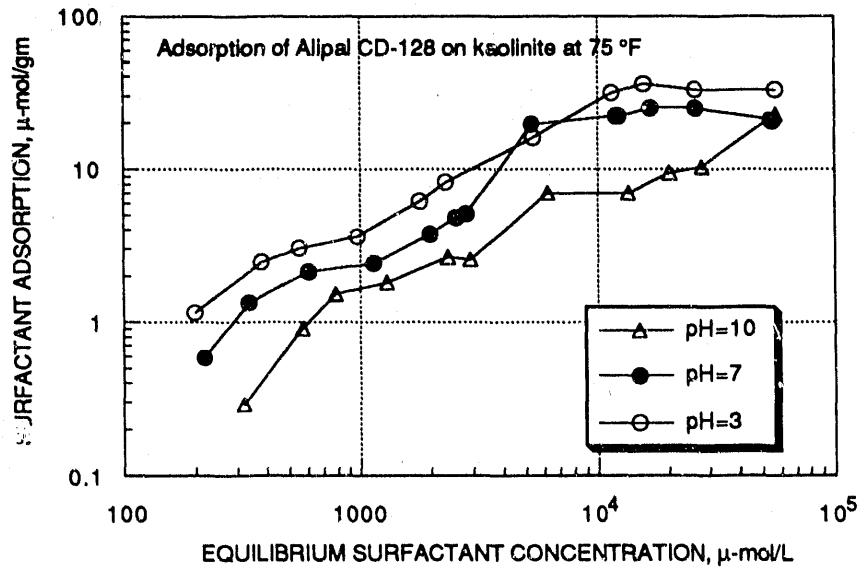

FIGURE C-3. - Effect of pH on Alipal CD-128 adsorption on kaolinite.

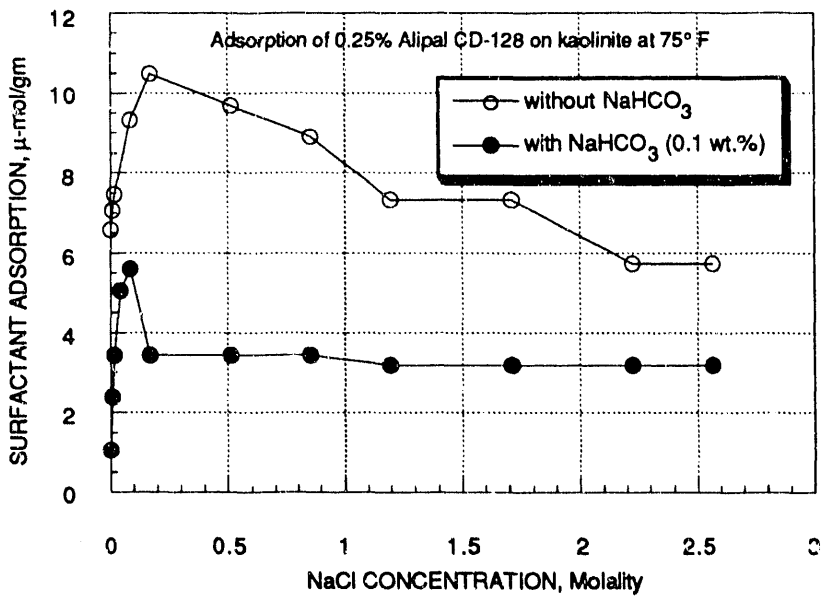

FIGURE C-4. - Alkaline effect of Alipal CD-128 adsorption on kaolinite.

END

DATE FILMED

06 / 20 / 91